Data and analysis for the CODATA 2017 special fundamental constants adjustment

OPEN ACCESS
IOP Publishing | Bureau International des Poids et Mesures
Metrologia

Metrologia **55** (2018) 125–146
https://doi.org/10.1088/1681-7575/aa99bc

Data and analysis for the CODATA 2017 special fundamental constants adjustment*

Peter J Mohr, David B Newell, Barry N Taylor and Eite Tiesinga

National Institute of Standards and Technology, Gaithersburg, MD 20899-8420, United States of America

E-mail: mohr@nist.gov, dnewell@nist.gov, barry.taylor@nist.gov and eite.tiesinga@nist.gov

Received 2 August 2017, revised 8 November 2017
Accepted for publication 10 November 2017
Published 24 January 2018

Abstract

The special least-squares adjustment of the values of the fundamental constants, carried out by the Committee on Data for Science and Technology (CODATA) in the summer of 2017, is described in detail. It is based on all relevant data available by 1 July 2017. The purpose of this adjustment is to determine the numerical values of the Planck constant h, elementary charge e, Boltzmann constant k, and Avogadro constant N_A for the revised SI expected to be established by the 26th General Conference on Weights and Measures when it convenes on 13–16 November 2018.

Keywords: International System of Units, fundamental constants, redefinition of the SI

(Some figures may appear in colour only in the online journal)

1. Introduction

The 26th General Conference on Weights and Measures (CGPM) is expected to establish at its meeting on 13–16 November 2018 a revised International System of Units (SI) based in part on exact numerical values of the Planck constant h, elementary charge e, Boltzmann constant k, and Avogadro constant N_A. To this end, at the invitation of the CGPM (CGPM 2011), the Committee on Data for Science and Technology (CODATA), through its Task Group on Fundamental Constants (the Task Group), carried out a special least-squares adjustment of the values of the fundamental physical constants during the summer of 2017. The required numerical values of h, e, k, and N_A resulting from that adjustment are reported by the Task Group (Newell *et al* 2018). Here we describe the data and analysis underlying the 2017 Special Adjustment.

In keeping with the request of the International Committee for Weights and Measures (CIPM), data to be considered for the adjustment had to be published in a refereed journal or accepted for publication by 1 July 2017 (CIPM 2015). The procedures used for the 2017 Special Adjustment are the same as those used for the 2014 regularly scheduled CODATA adjustment and its 1998, 2002, 2006, and 2010 predecessors (Mohr and Taylor 2000, 2005, Mohr *et al* 2008a, 2008b, 2012a, 2012b, 2016a, 2016b).

2. Least-squares adjustments

The method of least-squares as used by the Task Group is discussed in detail in appendix E of CODATA-98. A few key points are as follows.

The numerical *input data* for an adjustment, obtained from experiment or theory, are expressed in terms of an independent set of quantities called *adjusted constants*. These are the variables of the adjustment and the equations that relate

* This report was prepared by the authors under the auspices of the Committee on Data for Science and Technology CODATA Task Group on Fundamental Constants. The members of the task group are F Cabiati, Istituto Nazionale di Ricerca Metrologica, Italy; J Fischer, Physikalisch-Technische Bundesanstalt, Germany; K Fujii, National Metrology Institute of Japan, Japan; S G Karshenboim, Pulkovo Observatory, Russian Federation and Ludwig-Maximilians-Universität, Germany; H S Margolis, National Phyiscal Laboratory, United Kingdom; E de Mirandés, Bureau international des poids et mesures; P J Mohr, National Institute of Standards and Technology, United States of America; D B Newell, National Institute of Standards and Technology, United States of America; F Nez, Laboratoire Kastler-Brossel, France; K Pachucki, University of Warsaw, Poland; T J Quinn, Bureau international des poids et mesures; B N Taylor, National Institute of Standards and Technology, United States of America; M Wang, Chinese Academy of Sciences, People's Republic of China; B M Wood, National Research Council, Canada; Z Zhang, National Institute of Metrology, People's Republic of China.

Table 1. Some exact quantities relevant to the 2017 adjustment.

Quantity	Symbol	Value
Speed of light in vacuum	c, c_0	299 792 458 m s^{-1}
Magnetic constant	μ_0	$4\pi \times 10^{-7}$ N $A^{-2} = 12.566\,370\,614... \times 10^{-7}$ N A^{-2}
Electric constant	ϵ_0	$(\mu_0 c^2)^{-1} = 8.854\,187\,817...\times 10^{-12}$ F m^{-1}
Molar mass of ^{12}C	$M(^{12}\mathrm{C})$	12×10^{-3} kg mol^{-1}
Molar mass constant	M_u	$M(^{12}\mathrm{C})/12 = 10^{-3}$ kg mol^{-1}
Relative atomic mass of ^{12}C	$A_r(^{12}\mathrm{C})$	12
Conventional value of Josephson constant	K_{J-90}	483 597.9 GHz V^{-1}
Conventional value of von Klitzing constant	R_{K-90}	25 812.807 Ω

the input data to the adjusted constants are called *observational equations*. The standard uncertainties of the input data and the covariances among the data, if any, are also required since they determine the weights of the input data.

An adjustment is characterized by the number of input data N, number of adjusted constants M, degrees of freedom $\nu = N - M$, statistic χ^2, probability $p\,(\chi^2|\nu)$ of obtaining an observed value of χ^2 by chance that large or larger for the given value of ν, and Birge ratio $R_B = \sqrt{\chi^2/\nu}$.

The normalized residual of the ith input datum $r_i = (x_i - \langle x_i \rangle)/u_i$, where x_i is the input datum, $\langle x_i \rangle$ its adjusted value, and u_i its standard uncertainty, is a measure of how well that datum agrees with other data. A value larger than 2 is generally viewed as a cause for concern and may require increasing the uncertainties of some input data by a multiplicative expansion factor.

The *self-sensitivity coefficient* S_c of an input datum is a measure of the influence of that datum on the adjustment. As discussed in CODATA-98, it should be no less than 0.01, or 1%, for the input datum to be included in the final adjustment on which recommended values of constants are based. However, the exclusion rule for a datum is not followed if, for example, a datum with $S_c < 0.01$ is part of a group of data obtained in a given experiment where most of the other data have self-sensitivity coefficients > 0.01. This 1% cutoff implies the input datum's uncertainty should be no more than about a factor of 10 larger than the uncertainty of the adjusted value of the quantity of which the datum is a particular example. That uncertainty follows from the datum's observational equation evaluated with the least-squares adjusted values of the adjusted constants on which the observational equation depends (see CODATA-98, column 1 of p 358 and of p 483 for further discussion).

3. Review of data

A list of the Symbols and Abbreviations used in this report is given at its end prior to the list of references. This list should be consulted as needed since to keep this report concise, the listed items are in general not fully defined in the text. Further, for the same reason, we sometimes refer the reader to a particular table in CODATA-14 rather than repeat it in this paper.

As in past CODATA adjustments, the uncertainty of a theoretical expression is taken into account by including in the expression an additive correction δ. Each such δ is taken as an adjusted constant and is included as an input datum with initial value zero but with an uncertainty equal to that of its corresponding theoretical expression. If corrections are correlated due to common uncertainty sources, the correlations are taken into account.

The purpose of the CODATA 2017 Special Adjustment is to obtain best numerical values for h, e, k, and N_A, not to provide a complete set of recommended values to replace the 2014 set. Nevertheless, to maintain the continuity of CODATA adjustments and to simplify the comparison of the CODATA 2017 Special Adjustment with the CODATA 2014 regular adjustment, the starting point of the 2017 Special Adjustment is the input data included in the final adjustment on which the 2014 CODATA recommended values are based. Consequently, the 22 input data omitted from that final adjustment because of their low weight are not considered for inclusion in the 2017 Special Adjustment. The only other data not considered are four cyclotron frequency ratios that have been superseded by a new atomic mass evaluation, and measurements of the Newtonian constant of gravitation G. The latter data are treated separately in CODATA adjustments because there is no known relationship between G and any other constant, and because the G data are independent of all other input data. Although our data review focuses on the new data, the data used in the 2014 final adjustment are duly noted. For details, including references, CODATA-14 and earlier CODATA reports should be consulted; in general only references to new work are given in this report.

3.1. Special quantities and units

Table 1 recalls a number of familiar, exactly-known constants relevant to the 2017 Special Adjustment. It is subject to modification after redefinition of the SI.

3.2. Data that determine the Rydberg constant R_∞

The Rydberg constant, which has one of the smallest relative uncertainties u_r of any measured constant, plays an important role in the 2017 Special Adjustment. It is obtained by equating measured transition frequencies in hydrogen (H) and Deuterium (D) with their theoretical expressions.

Table 2 gives the principal input data that determine the 2017 Special Adjustment value of R_∞ and table 3 gives their correlation coefficients. The adjusted constants in terms of which the R_∞ input data in table 2 are expressed are given in table XXV of CODATA-14 and the observational equation for

Table 2. Summary of principal input data relevant to the Rydberg constant R_∞ for the CODATA 2017 Special Adjustment.

Item number	Input datum	Value	Relative standard uncertainty[a] u_r	Identification
*A*1	$\delta_H(1S_{1/2})$	0.0(2.3) kHz	$[7.1 \times 10^{-13}]$	Theory
*A*2	$\delta_H(2S_{1/2})$	0.00(29) kHz	$[3.6 \times 10^{-13}]$	Theory
*A*3	$\delta_H(3S_{1/2})$	0.000(87) kHz	$[2.4 \times 10^{-13}]$	Theory
*A*4	$\delta_H(4S_{1/2})$	0.000(37) kHz	$[1.8 \times 10^{-13}]$	Theory
*A*5	$\delta_H(6S_{1/2})$	0.000(14) kHz	$[1.6 \times 10^{-13}]$	Theory
*A*6	$\delta_H(8S_{1/2})$	0.0000(61) kHz	$[1.2 \times 10^{-13}]$	Theory
*A*7	$\delta_H(2P_{1/2})$	0.000(28) kHz	$[3.4 \times 10^{-14}]$	Theory
*A*8	$\delta_H(4P_{1/2})$	0.0000(38) kHz	$[1.9 \times 10^{-14}]$	Theory
*A*9	$\delta_H(2P_{3/2})$	0.000(28) kHz	$[3.4 \times 10^{-14}]$	Theory
*A*10	$\delta_H(4P_{3/2})$	0.0000(38) kHz	$[1.9 \times 10^{-14}]$	Theory
*A*11	$\delta_H(8D_{3/2})$	0.000 00(44) kHz	$[8.5 \times 10^{-15}]$	Theory
*A*12	$\delta_H(12D_{3/2})$	0.000 00(13) kHz	$[5.7 \times 10^{-15}]$	Theory
*A*13	$\delta_H(4D_{5/2})$	0.0000(35) kHz	$[1.7 \times 10^{-14}]$	Theory
*A*14	$\delta_H(6D_{5/2})$	0.0000(10) kHz	$[1.1 \times 10^{-14}]$	Theory
*A*15	$\delta_H(8D_{5/2})$	0.000 00(44) kHz	$[8.5 \times 10^{-15}]$	Theory
*A*16	$\delta_H(12D_{5/2})$	0.000 00(13) kHz	$[5.7 \times 10^{-15}]$	Theory
*A*17	$\delta_D(1S_{1/2})$	0.0(2.2) kHz	$[6.8 \times 10^{-13}]$	Theory
*A*18	$\delta_D(2S_{1/2})$	0.00(28) kHz	$[3.4 \times 10^{-13}]$	Theory
*A*19	$\delta_D(4S_{1/2})$	0.000(35) kHz	$[1.7 \times 10^{-13}]$	Theory
*A*20	$\delta_D(8S_{1/2})$	0.0000(59) kHz	$[1.2 \times 10^{-13}]$	Theory
*A*21	$\delta_D(8D_{3/2})$	0.000 00(44) kHz	$[8.5 \times 10^{-15}]$	Theory
*A*22	$\delta_D(12D_{3/2})$	0.000 00(13) kHz	$[5.6 \times 10^{-15}]$	Theory
*A*23	$\delta_D(4D_{5/2})$	0.0000(35) kHz	$[1.7 \times 10^{-14}]$	Theory
*A*24	$\delta_D(8D_{5/2})$	0.000 00(44) kHz	$[8.5 \times 10^{-15}]$	Theory
*A*25	$\delta_D(12D_{5/2})$	0.000 00(13) kHz	$[5.7 \times 10^{-15}]$	Theory
*A*26.1	$\nu_H(1S_{1/2} - 2S_{1/2})$	2 466 061 413 187.035(10) kHz	4.2×10^{-15}	MPQ-11
*A*26.2	$\nu_H(1S_{1/2} - 2S_{1/2})$	2 466 061 413 187.018(11) kHz	4.4×10^{-15}	MPQ-13
*A*27.1	$\nu_H(1S_{1/2} - 3S_{1/2})$	2 922 743 278 678(13) kHz	4.4×10^{-12}	LKB-10
*A*27.2	$\nu_H(1S_{1/2} - 3S_{1/2})$	2 922 743 278 659(17) kHz	5.8×10^{-12}	MPQ-16
*A*28	$\nu_H(2S_{1/2} - 8S_{1/2})$	770 649 350 012.0(8.6) kHz	1.1×10^{-11}	LK/SY-97
*A*29	$\nu_H(2S_{1/2} - 8D_{3/2})$	770 649 504 450.0(8.3) kHz	1.1×10^{-11}	LK/SY-97
*A*30	$\nu_H(2S_{1/2} - 8D_{5/2})$	770 649 561 584.2(6.4) kHz	8.3×10^{-12}	LK/SY-97
*A*31	$\nu_H(2S_{1/2} - 12D_{3/2})$	799 191 710 472.7(9.4) kHz	1.2×10^{-11}	LK/SY-98
*A*32	$\nu_H(2S_{1/2} - 12D_{5/2})$	799 191 727 403.7(7.0) kHz	8.7×10^{-12}	LK/SY-98
*A*33	$\nu_H(2S_{1/2} - 4S_{1/2}) - \frac{1}{4}\nu_H(1S_{1/2} - 2S_{1/2})$	4 797 338(10) kHz	2.1×10^{-6}	MPQ-95
*A*34	$\nu_H(2S_{1/2} - 4D_{5/2}) - \frac{1}{4}\nu_H(1S_{1/2} - 2S_{1/2})$	6 490 144(24) kHz	3.7×10^{-6}	MPQ-95
*A*35	$\nu_H(2S_{1/2} - 6S_{1/2}) - \frac{1}{4}\nu_H(1S_{1/2} - 3S_{1/2})$	4 197 604(21) kHz	4.9×10^{-6}	LKB-96
*A*36	$\nu_H(2S_{1/2} - 6D_{5/2}) - \frac{1}{4}\nu_H(1S_{1/2} - 3S_{1/2})$	4 699 099(10) kHz	2.2×10^{-6}	LKB-96
*A*37	$\nu_H(2S_{1/2} - 4P_{1/2}) - \frac{1}{4}\nu_H(1S_{1/2} - 2S_{1/2})$	4 664 269(15) kHz	3.2×10^{-6}	YaleU-95
*A*38	$\nu_H(2S_{1/2} - 4P_{3/2}) - \frac{1}{4}\nu_H(1S_{1/2} - 2S_{1/2})$	6 035 373(10) kHz	1.7×10^{-6}	YaleU-95
*A*39	$\nu_H(2S_{1/2} - 2P_{3/2})$	9 911 200(12) kHz	1.2×10^{-6}	HarvU-94
*A*40.1	$\nu_H(2P_{1/2} - 2S_{1/2})$	1 057 845.0(9.0) kHz	8.5×10^{-6}	HarvU-86
*A*40.2	$\nu_H(2P_{1/2} - 2S_{1/2})$	1 057 862(20) kHz	1.9×10^{-5}	USus-79
*A*41	$\nu_D(2S_{1/2} - 8S_{1/2})$	770 859 041 245.7(6.9) kHz	8.9×10^{-12}	LK/SY-97
*A*44	$\nu_D(2S_{1/2} - 8D_{3/2})$	770 859 195 701.8(6.3) kHz	8.2×10^{-12}	LK/SY-97
*A*43	$\nu_D(2S_{1/2} - 8D_{5/2})$	770 859 252 849.5(5.9) kHz	7.7×10^{-12}	LK/SY-97
*A*44	$\nu_D(2S_{1/2} - 12D_{3/2})$	799 409 168 038.0(8.6) kHz	1.1×10^{-11}	LK/SY-98
*A*45	$\nu_D(2S_{1/2} - 12D_{5/2})$	799 409 184 966.8(6.8) kHz	8.5×10^{-12}	LK/SY-98
*A*46	$\nu_D(2S_{1/2} - 4S_{1/2}) - \frac{1}{4}\nu_D(1S_{1/2} - 2S_{1/2})$	4 801 693(20) kHz	4.2×10^{-6}	MPQ-95
*A*47	$\nu_D(2S_{1/2} - 4D_{5/2}) - \frac{1}{4}\nu_D(1S_{1/2} - 2S_{1/2})$	6 494 841(41) kHz	6.3×10^{-6}	MPQ-95
*A*48	$\nu_D(1S_{1/2} - 2S_{1/2}) - \nu_H(1S_{1/2} - 2S_{1/2})$	670 994 334.606(15) kHz	2.2×10^{-11}	MPQ-10
*A*49	r_p	0.879(11) fm	1.3×10^{-2}	rp-14
*A*50	r_d	2.130(10) fm	4.7×10^{-3}	rd-98

[a] The values in brackets are relative to the frequency equivalent of the binding energy of the indicated level.

Table 3. Correlation coefficients with $|r(x_i, x_j)| \geqslant 0.0001$ of the input data related to R_∞ in table 2. For simplicity, the two items of data to which a particular correlation coefficient corresponds are identified by their item numbers in table 2.

$r(A1, A2) = 0.9895$	$r(A5, A20) = 0.5440$	$r(A21, A22) = 0.0002$	$r(A31, A36) = 0.0412$
$r(A1, A3) = 0.9888$	$r(A6, A17) = 0.7344$	$r(A23, A24) = 0.0001$	$r(A31, A41) = 0.1127$
$r(A1, A4) = 0.9859$	$r(A6, A18) = 0.7342$	$r(A23, A25) = 0.0001$	$r(A31, A43) = 0.1305$
$r(A1, A5) = 0.7465$	$r(A6, A19) = 0.7313$	$r(A24, A25) = 0.0002$	$r(A31, A44) = 0.0901$
$r(A1, A6) = 0.7451$	$r(A6, A20) = 0.9918$	$r(A26.1, A26.2) = 0.7069$	$r(A31, A45) = 0.1136$
$r(A1, A17) = 0.9857$	$r(A11, A12) = 0.0006$	$r(A28, A29) = 0.3478$	$r(A32, A35) = 0.0278$
$r(A1, A18) = 0.9752$	$r(A11, A21) = 0.9999$	$r(A28, A30) = 0.4532$	$r(A32, A36) = 0.0553$
$r(A1, A19) = 0.9714$	$r(A11, A22) = 0.0003$	$r(A28, A31) = 0.0899$	$r(A32, A41) = 0.1512$
$r(A1, A20) = 0.7212$	$r(A12, A21) = 0.0003$	$r(A28, A32) = 0.1206$	$r(A32, A43) = 0.1750$
$r(A2, A3) = 0.9885$	$r(A12, A22) = 0.9999$	$r(A28, A35) = 0.0225$	$r(A32, A44) = 0.1209$
$r(A2, A4) = 0.9856$	$r(A13, A14) = 0.0006$	$r(A28, A36) = 0.0448$	$r(A32, A45) = 0.1524$
$r(A2, A5) = 0.7463$	$r(A13, A15) = 0.0006$	$r(A28, A41) = 0.1225$	$r(A33, A34) = 0.1049$
$r(A2, A6) = 0.7449$	$r(A13, A16) = 0.0006$	$r(A28, A43) = 0.1419$	$r(A33, A46) = 0.2095$
$r(A2, A17) = 0.9752$	$r(A13, A23) = 0.9999$	$r(A28, A44) = 0.0980$	$r(A33, A47) = 0.0404$
$r(A2, A18) = 0.9857$	$r(A13, A24) = 0.0003$	$r(A28, A45) = 0.1235$	$r(A34, A46) = 0.0271$
$r(A2, A19) = 0.9711$	$r(A13, A25) = 0.0003$	$r(A29, A30) = 0.4696$	$r(A34, A47) = 0.0467$
$r(A2, A20) = 0.7210$	$r(A14, A15) = 0.0006$	$r(A29, A31) = 0.0934$	$r(A35, A36) = 0.1412$
$r(A3, A4) = 0.9849$	$r(A14, A16) = 0.0006$	$r(A29, A32) = 0.1253$	$r(A35, A41) = 0.0282$
$r(A3, A5) = 0.7458$	$r(A14, A23) = 0.0003$	$r(A29, A35) = 0.0234$	$r(A35, A43) = 0.0327$
$r(A3, A6) = 0.7444$	$r(A14, A24) = 0.0003$	$r(A29, A36) = 0.0466$	$r(A35, A44) = 0.0226$
$r(A3, A17) = 0.9746$	$r(A14, A25) = 0.0003$	$r(A29, A41) = 0.1273$	$r(A35, A45) = 0.0284$
$r(A3, A18) = 0.9743$	$r(A15, A16) = 0.0006$	$r(A29, A43) = 0.1475$	$r(A36, A41) = 0.0561$
$r(A3, A19) = 0.9705$	$r(A15, A23) = 0.0003$	$r(A29, A44) = 0.1019$	$r(A36, A43) = 0.0650$
$r(A3, A20) = 0.7205$	$r(A15, A24) = 0.9999$	$r(A29, A45) = 0.1284$	$r(A36, A44) = 0.0449$
$r(A4, A5) = 0.7436$	$r(A15, A25) = 0.0003$	$r(A30, A31) = 0.1209$	$r(A36, A45) = 0.0566$
$r(A4, A6) = 0.7422$	$r(A16, A23) = 0.0003$	$r(A30, A32) = 0.1622$	$r(A37, A38) = 0.0834$
$r(A4, A17) = 0.9717$	$r(A16, A24) = 0.0003$	$r(A30, A35) = 0.0303$	$r(A41, A43) = 0.6117$
$r(A4, A18) = 0.9714$	$r(A16, A25) = 0.9999$	$r(A30, A36) = 0.0602$	$r(A41, A44) = 0.1229$
$r(A4, A19) = 0.9858$	$r(A17, A18) = 0.9894$	$r(A30, A41) = 0.1648$	$r(A41, A45) = 0.1548$
$r(A4, A20) = 0.7184$	$r(A17, A19) = 0.9855$	$r(A30, A43) = 0.1908$	$r(A43, A44) = 0.1423$
$r(A5, A6) = 0.5620$	$r(A17, A20) = 0.7317$	$r(A30, A44) = 0.1319$	$r(A43, A45) = 0.1793$
$r(A5, A17) = 0.7358$	$r(A18, A19) = 0.9852$	$r(A30, A45) = 0.1662$	$r(A44, A45) = 0.5224$
$r(A5, A18) = 0.7355$	$r(A18, A20) = 0.7315$	$r(A31, A32) = 0.4750$	$r(A46, A47) = 0.0110$
$r(A5, A19) = 0.7326$	$r(A19, A20) = 0.7286$	$r(A31, A35) = 0.0207$	

each input datum may be found in table XXIII of CODATA-14; thus they need not be repeated here. It should be recalled that the symbol $\doteq$ in an observational equation indicates that an input datum on the left-hand side is ideally given by the expression on the right-hand side containing adjusted constants. But because the equation is one of an overdetermined set that relates a datum to adjusted constants, the two sides are not necessarily equal.

The discussion of the principal data that determine R_∞ in table 2 follows the order in which they are listed. Items *A*1-*A*25 are the additive corrections for the theoretical expressions of the indicated H and D energy levels and items *A*26.1-*A*48 are the experimentally measured H and D transition frequencies. Items *A*49 and *A*50 are the root-mean-square (rms) electric charge radii of the proton r_p and deuteron r_d required by the theory and obtained from elastic electron scattering data. Differences between table 2 and the corresponding table XVI in CODATA-14 (and hence to some extent between table 3 and its corresponding table XVII in CODATA-14) are as follows.

There are a few changes in the theory of the H and D energy levels as given in CODATA-14 but none of major consequence; none of the uncertainties of the additive corrections to the theory, items *A*1-*A*25 of table 2, have changed significantly from their 2014 values. This also applies to their correlation coefficients given in table 3. The changes in the theory are (i) incorporation of the $\delta^2 B_{60}$ contribution to b_L in equation (67) of CODATA-10 based on our reanalysis of the paper by Jentschura (2006); (ii) inclusion of improved relativistic nuclear recoil corrections and the effect of finite nuclear size on them calculated by Yerokhin and Shabaev (2016) and Yerokhin and Shabaev (2015); and (iii) addition of a contribution from light-by-light scattering diagrams to the coefficient B_{61} in equation (55) of CODATA-14 calculated by Czarnecki and Szafron (2016) that reduces the $\nu_H(1S_{1/2} - 2S_{1/2})$ theoretical transition frequency by about 281 Hz.

The only new frequency in table 2 is item *A*27.2 for the $\nu_H(1S_{1/2} - 3S_{1/2})$ transition from the group at the MPQ, Garching, as reported by Yost *et al* (2016). The frequency was determined using two-photon direct frequency comb spectroscopy, or DFCS. This technique employs the high peak intensities of the ultra-short pulse trains of an optical comb to generate the required short-wavelength radiation, in this case 205 nm. However, in contrast to two-photon spectroscopy using counter propagating continuous-wave (cw) radiation to eliminate first-order Doppler broadening, in DFCS such broadening is not completely eliminated because of varying frequency across the pulses, or 'chirp'. The experimenters thoroughly investigated this systematic effect and developed techniques to mitigate it. The net correction to their initially measured frequency is 80.9 kHz and the three largest uncertainty components contributing to the 17 kHz total uncertainty are, in kHz, 13 for second-order Doppler broadening, 8.4 for the frequency measurement, and 6.3 for pressure shift.

Table 4. Summary of principal input data relevant to the fundamental constants other than R_∞ for the CODATA 2017 Special Adjustment.

Item number	Input datum	Value	Relative standard uncertainty[a] u_r	Identification
*B*1	$A_r(n)$	1.008 664 915 82(49)	4.9×10^{-10}	AME-16
*B*2	$A_r(^1H)$	1.007 825 032 241(94)	9.3×10^{-11}	AME-16
*B*3	$\Delta E_B(^1H^+)/hc$	1.096 787 717 4307(10) $\times 10^7$ m^{-1}	9.1×10^{-13}	ASD-17
*B*4	$A_r(^2H)$	2.014 101 778 11(12)	6.0×10^{-11}	AME-16
*B*5	$\Delta E_B(^2H^+)/hc$	1.097 086 145 5299(10) $\times 10^7$ m^{-1}	9.1×10^{-13}	ASD-17
*B*6	$A_r(^3H)$	3.016 049 281 98(23)	7.7×10^{-11}	AME-16
*B*7	$\Delta E_B(^3H^+)/hc$	1.097 185 4390(13) $\times 10^7$ m^{-1}	1.2×10^{-9}	ASD-17
*B*8	$A_r(^3He)$	3.016 029 322 65(22)	7.3×10^{-11}	AME-16
*B*9	$\Delta E_B(^3He^{2+})/hc$	6.371 894 047(11) $\times 10^7$ m^{-1}	1.8×10^{-9}	ASD-17
*B*10	$A_r(^4He)$	4.002 603 254 130(63)	1.6×10^{-11}	AME-16
*B*11	$\Delta E_B(^4He^{2+})/hc$	6.372 195 4487(28) $\times 10^7$ m^{-1}	4.4×10^{-10}	ASD-17
*B*12	$\omega_c(^{12}C^{6+})/\omega_c(p)$	0.503 776 367 662(17)	3.3×10^{-11}	MPIK-17
*B*13	$\Delta E_B(^{12}C^{6+})/hc$	83.083 957(72) $\times 10^7$ m^{-1}	8.7×10^{-7}	ASD-17
*B*14	$\omega_s(^{12}C^{5+})/\omega_c(^{12}C^{5+})$	4 376.210 500 87(12)	2.8×10^{-11}	MPIK-15
*B*15	$\Delta E_B(^{12}C^{5+})/hc$	43.563 340(72) $\times 10^7$ m^{-1}	1.7×10^{-6}	ASD-17
*B*16	δ_C	0.0(2.5) $\times 10^{-11}$	[1.3×10^{-11}]	Theory
*B*17	$\omega_s(^{28}Si^{13+})/\omega_c(^{28}Si^{13+})$	3 912.866 064 84(19)	4.8×10^{-11}	MPIK-15
*B*18	$A_r(^{28}Si)$	27.976 926 534 99(52)	1.9×10^{-11}	AME-16
*B*19	$\Delta E_B(^{28}Si^{13+})/hc$	420.608(19) $\times 10^7$ m^{-1}	4.4×10^{-5}	ASD-17
*B*20	δ_{Si}	0.0(1.7) $\times 10^{-9}$	[8.3×10^{-10}]	Theory
*B*21	a_e	1.159 652 180 73(28) $\times 10^{-3}$	2.4×10^{-10}	HarvU-08
*B*22	δ_e	0.000(21) $\times 10^{-12}$	[0.18×10^{-10}]	Theory
*B*23	$\overline{R}$	0.003 707 2063(20)	5.4×10^{-7}	BNL-06
*B*24	ν(58 MHz)	627 994.77(14) kHz	2.2×10^{-7}	LAMPF-82
*B*25	ν(72 MHz)	668 223 166(57) Hz	8.6×10^{-8}	LAMPF-99
*B*26.1	$\Delta\nu_{Mu}$	4 463 302.88(16) kHz	3.6×10^{-8}	LAMPF-82
*B*26.2	$\Delta\nu_{Mu}$	4 463 302 765(53) Hz	1.2×10^{-8}	LAMPF-99
*B*27	δ_{Mu}	0(85) Hz	[1.9×10^{-8}]	Theory
*B*28	μ_p/μ_N	2.792 847 3498(93)	3.3×10^{-9}	UMZ-14
*B*29	$\mu_e(H)/\mu_p(H)$	−658.210 7058(66)	1.0×10^{-8}	MIT-72
*B*30	$\mu_d(D)/\mu_e(D)$	−4.664 345 392(50) $\times 10^{-4}$	1.1×10^{-8}	MIT-84
*B*31	$\mu_e(H)/\mu'_p$	−658.215 9430(72)	1.1×10^{-8}	MIT-77
*B*32	μ'_h/μ'_p	−0.761 786 1313(33)	4.3×10^{-9}	NPL-93
*B*33	μ_n/μ'_p	−0.684 996 94(16)	2.4×10^{-7}	ILL-79
*B*34.1	$\mu_p(HD)/\mu_d(HD)$	3.257 199 531(29)	8.9×10^{-9}	StPtrsb-03
*B*34.2	$\mu_p(HD)/\mu_d(HD)$	3.257 199 514(21)	6.6×10^{-9}	WarsU-12
*B*35	$\mu_t(HT)/\mu_p(HT)$	1.066 639 8933(21)	2.0×10^{-9}	StPtrsb-11
*B*36	σ_{dp}	20.20(2) $\times 10^{-9}$		Theory
*B*37	σ_{tp}	24.14(2) $\times 10^{-9}$		Theory
*B*38.1	h	6.626 068 91(58) $\times 10^{-34}$ J s	8.7×10^{-8}	NIST-98
*B*38.2	h	6.626 069 36(38) $\times 10^{-34}$ J s	5.7×10^{-8}	NIST-15
*B*38.3	h	6.626 069 934(88) $\times 10^{-34}$ J s	1.3×10^{-8}	NIST-17
*B*38.4	h	6.626 070 133(60) $\times 10^{-34}$ J s	9.1×10^{-9}	NRC-17
*B*38.5	h	6.626 070 40(38) $\times 10^{-34}$ J s	5.7×10^{-8}	LNE-17
*B*39	$h/m(^{87}Rb)$	4.591 359 2729(57) $\times 10^{-9}$ m^2 s^{-1}	1.2×10^{-9}	LKB-11
*B*40	$A_r(^{87}Rb)$	86.909 180 5312(65)	7.4×10^{-11}	AME-16
*B*41	$1 - d_{220}(W17)/d_{220}(ILL)$	$-8(22) \times 10^{-9}$		NIST-99
*B*42	$1 - d_{220}(MO^*)/d_{220}(ILL)$	$86(27) \times 10^{-9}$		NIST-99
*B*43	$1 - d_{220}(NR3)/d_{220}(ILL)$	$33(22) \times 10^{-9}$		NIST-99
*B*44	$1 - d_{220}(N)/d_{220}(W17)$	$7(22) \times 10^{-9}$		NIST-97
*B*45	$d_{220}(W4.2a)/d_{220}(W04) - 1$	$-1(21) \times 10^{-9}$		PTB-98
*B*46.1	$d_{220}(W17)/d_{220}(W04) - 1$	$22(22) \times 10^{-9}$		PTB-98
*B*46.2	$d_{220}(W17)/d_{220}(W04) - 1$	$11(21) \times 10^{-9}$		NIST-06
*B*47	$d_{220}(MO^*)/d_{220}(W04) - 1$	$-103(28) \times 10^{-9}$		PTB-98
*B*48.1	$d_{220}(NR3)/d_{220}(W04) - 1$	$-23(21) \times 10^{-9}$		PTB-98
*B*48.2	$d_{220}(NR3)/d_{220}(W04) - 1$	$-11(21) \times 10^{-9}$		NIST-06

(*Continued*)

Table 4. (Continued)

Item number	Input datum	Value	Relative standard uncertainty[a] u_r	Identification
*B*49	$d_{220}/d_{220}(\mathrm{W04}) - 1$	$10(11) \times 10^{-9}$		PTB-03
*B*50	$d_{220}(\mathrm{NR4})/d_{220}(\mathrm{W04}) - 1$	$25(21) \times 10^{-9}$		NIST-06
*B*51	$d_{220}(\mathrm{MO}^*)$	192 015.5508(42) fm	2.2×10^{-8}	INRIM-08
*B*52	$d_{220}(\mathrm{W04})$	192 015.5702(29) fm	1.5×10^{-8}	INRIM-09
*B*53.1	$d_{220}(\mathrm{W4.2a})$	192 015.5691(29) fm	1.5×10^{-8}	INRIM-09
*B*53.2	$d_{220}(\mathrm{W4.2a})$	192 015.563(12) fm	6.2×10^{-8}	PTB-81
*B*54.1	N_A	$6.022\,140\,95(18) \times 10^{23}$ mol^{-1}	3.0×10^{-8}	IAC-11
*B*54.2	N_A	$6.022\,140\,70(12) \times 10^{23}$ mol^{-1}	2.0×10^{-8}	IAC-15
*B*54.3	N_A	$6.022\,140\,526(70) \times 10^{23}$ mol^{-1}	1.2×10^{-8}	IAC-17
*B*54.4	N_A	$6.022\,140\,78(15) \times 10^{23}$ mol^{-1}	2.4×10^{-8}	NMIJ-17
*B*55.1	R	8.314 470(15) J mol^{-1} K^{-1}	1.8×10^{-6}	NIST-88
*B*55.2	R	8.314 467(23) J mol^{-1} K^{-1}	2.7×10^{-6}	LNE-09
*B*55.3	R	8.314 468(26) J mol^{-1} K^{-1}	3.2×10^{-6}	NPL-10
*B*55.4	R	8.314 455(12) J mol^{-1} K^{-1}	1.4×10^{-6}	LNE-11
*B*55.5	R	8.314 4615(84) J mol^{-1} K^{-1}	1.0×10^{-6}	LNE-15
*B*55.6	R	8.314 4743(88) J mol^{-1} K^{-1}	1.1×10^{-6}	INRIM-15
*B*55.7	R	8.314 459(17) J mol^{-1} K^{-1}	2.0×10^{-6}	NIM-17
*B*55.8	R	8.314 4603(58) J mol^{-1} K^{-1}	7.0×10^{-7}	NPL-17
*B*55.9	R	8.314 4614(50) J mol^{-1} K^{-1}	6.0×10^{-7}	LNE-17
*B*55.10	R	8.314 449(56) J mol^{-1} K^{-1}	6.7×10^{-6}	UVa/CEM-17
*B*56.1	k/h	$2.083\,6658(80) \times 10^{10}$ Hz K^{-1}	3.9×10^{-6}	NIM/NIST-15
*B*56.2	k/h	$2.083\,6630(56) \times 10^{10}$ Hz K^{-1}	2.7×10^{-6}	NIM/NIST-17
*B*56.3	k/h	$2.083\,653(10) \times 10^{10}$ Hz K^{-1}	5.0×10^{-6}	NIST-17
*B*57	$A_\epsilon(^4\mathrm{He})/R$	$6.221\,140(12) \times 10^{-8}$ m^3 K J^{-1}	1.9×10^{-6}	PTB-17
*B*58	$\alpha_0(^4\mathrm{He})/4\pi\epsilon_0 a_0^3$	1.383 760 77(14)	1.0×10^{-7}	Theory
*B*59	$\lambda(\mathrm{CuK}\alpha_1)/d_{220}(\mathrm{W4.2a})$	0.802 327 11(24)	3.0×10^{-7}	FSUJ/PTB-91
*B*60	$\lambda(\mathrm{CuK}\alpha_1)/d_{220}(\mathrm{N})$	0.802 328 04(77)	9.6×10^{-7}	NIST-73
*B*61	$\lambda(\mathrm{WK}\alpha_1)/d_{220}(\mathrm{N})$	0.108 852 175(98)	9.0×10^{-7}	NIST-79
*B*62	$\lambda(\mathrm{MoK}\alpha_1)/d_{220}(\mathrm{N})$	0.369 406 04(19)	5.3×10^{-7}	NIST-73

[a] The values in brackets are relative to the quantities $g(^{12}\mathrm{C}^{5+})$, $g(^{28}\mathrm{Si}^{13+})$, a_e, or $\Delta\nu_{\mathrm{Mu}}$ as appropriate.

Table 5. Correlation coefficients $|r(x_i, x_j)| \geqslant 0.001$ of the input data in table 4. For simplicity, the two items of data to which a particular correlation coefficient corresponds are identified by their item numbers in table 4.

$r(B1, B2) = -0.134$	$r(B18, B40) = 0.049$	$r(B45, B46.1) = 0.469$	$r(B55.2, B55.6) = 0.004$
$r(B1, B4) = 0.204$	$r(B24, B26.1) = 0.227$	$r(B45, B47) = 0.372$	$r(B55.2, B55.8) = 0.008$
$r(B1, B6) = 0.053$	$r(B25, B26.2) = 0.195$	$r(B45, B48.1) = 0.502$	$r(B55.2, B55.9) = 0.026$
$r(B1, B8) = 0.056$	$r(B38.1, B38.2) = 0.090$	$r(B46.1, B47) = 0.347$	$r(B55.3, B55.4) = 0.113$
$r(B1, B18) = -0.020$	$r(B41, B42) = 0.421$	$r(B46.1, B48.1) = 0.469$	$r(B55.3, B55.5) = 0.005$
$r(B1, B40) = -0.007$	$r(B41, B43) = 0.516$	$r(B46.2, B48.2) = 0.509$	$r(B55.3, B55.6) = 0.003$
$r(B2, B4) = 0.230$	$r(B41, B44) = -0.288$	$r(B46.2, B50) = 0.509$	$r(B55.3, B55.7) = 0.001$
$r(B2, B6) = 0.527$	$r(B41, B46.2) = -0.367$	$r(B47, B48.1) = 0.372$	$r(B55.3, B55.8) = 0.009$
$r(B2, B8) = 0.553$	$r(B41, B48.2) = 0.065$	$r(B48.2, B50) = 0.509$	$r(B55.3, B55.9) = 0.008$
$r(B2, B18) = 0.193$	$r(B41, B50) = 0.065$	$r(B54.1, B54.2) = 0.245$	$r(B55.4, B55.5) = 0.254$
$r(B2, B40) = 0.066$	$r(B42, B43) = 0.421$	$r(B54.1, B54.3) = 0.188$	$r(B55.4, B55.6) = 0.007$
$r(B4, B6) = 0.620$	$r(B42, B44) = 0.096$	$r(B54.1, B54.4) = 0.134$	$r(B55.4, B55.7) = 0.002$
$r(B4, B8) = 0.651$	$r(B42, B46.2) = 0.053$	$r(B54.2, B54.3) = 0.303$	$r(B55.4, B55.8) = 0.021$
$r(B4, B18) = 0.069$	$r(B42, B48.2) = 0.053$	$r(B54.2, B54.4) = 0.276$	$r(B55.4, B55.9) = 0.048$
$r(B4, B40) = 0.022$	$r(B42, B50) = 0.053$	$r(B54.3, B54.4) = 0.205$	$r(B55.5, B55.6) = 0.011$
$r(B6, B8) = 0.953$	$r(B43, B44) = 0.117$	$r(B55.1, B55.3) = 0.001$	$r(B55.5, B55.8) = 0.021$
$r(B6, B18) = 0.115$	$r(B43, B46.2) = 0.065$	$r(B55.1, B55.4) = 0.002$	$r(B55.5, B55.9) = 0.070$
$r(B6, B40) = 0.039$	$r(B43, B48.2) = -0.367$	$r(B55.1, B55.7) = 0.002$	$r(B55.6, B55.8) = 0.014$
$r(B8, B18) = 0.121$	$r(B43, B50) = 0.065$	$r(B55.1, B55.8) = 0.005$	$r(B55.6, B55.9) = 0.019$
$r(B8, B40) = 0.040$	$r(B44, B46.2) = 0.504$	$r(B55.2, B55.3) = 0.002$	$r(B55.7, B55.8) = 0.109$
$r(B14, B17) = 0.347$	$r(B44, B48.2) = 0.066$	$r(B55.2, B55.4) = 0.011$	$r(B55.8, B55.9) = 0.036$
$r(B16, B20) = 0.799$	$r(B44, B50) = 0.066$	$r(B55.2, B55.5) = 0.015$	

Table 6. Variables used in the least-squares adjustment of the constants. They are arguments of the functions on the right-hand side of the observational equations in table 7.

Adjusted constant	Symbol
Neutron relative atomic mass	$A_r(n)$
Electron relative atomic mass	$A_r(e)$
Proton relative atomic mass	$A_r(p)$
$^1H^+$ electron removal energy	$\Delta E_B(^1H^+)$
Deuteron relative atomic mass	$A_r(d)$
$^2H^+$ electron removal energy	$\Delta E_B(^2H^+)$
Triton relative atomic mass	$A_r(t)$
$^3H^+$ electron removal energy	$\Delta E_B(^3H^+)$
Helion relative atomic mass	$A_r(h)$
$^3He^+$ electron removal energy	$\Delta E_B(^3He^{2+})$
Alpha particle relative atomic mass	$A_r(\alpha)$
$^4He^{2+}$ electron removal energy	$\Delta E_B(^4He^{2+})$
$^{12}C^{6+}$ electron removal energy	$\Delta E_B(^{12}C^{6+})$
$^{12}C^{5+}$ electron removal energy	$\Delta E_B(^{12}C^{5+})$
Additive correction to $g_C(\alpha)$	δ_C
$^{28}Si^{13+}$ relative atomic mass	$A_r(^{28}Si^{13+})$
$^{28}Si^{13+}$ electron removal energy	$\Delta E_B(^{28}Si^{13+})$
Additive correction to $g_{Si}(\alpha)$	δ_{Si}
Fine-structure constant	α
Additive correction to a_e(th)	δ_e
Muon magnetic moment anomaly	a_μ
Electron-muon mass ratio	m_e/m_μ
Electron–proton magnetic moment ratio	μ_e/μ_p
Additive correction to $\Delta\nu_{Mu}$(th)	δ_{Mu}
Deuteron-electron magnetic moment ratio	μ_d/μ_e
Shielded helion to shielded proton magnetic moment ratio	μ'_h/μ'_p
Neutron to shielded proton magnetic moment ratio	μ_n/μ'_p
Shielding difference of d and p in HD	σ_{dp}
Triton-proton magnetic moment ratio	μ_t/μ_p
Shielding difference of t and p in HT	σ_{tp}
Electron to shielded proton magnetic moment ratio	μ_e/μ'_p
Planck constant	h
^{87}Rb relative atomic mass	$A_r(^{87}Rb)$
d_{220} of Si crystal WASO 17	d_{220}(W17)
d_{220} of Si crystal ILL	d_{220}(ILL)
d_{220} of Si crystal MO*	d_{220}(MO*)
d_{220} of Si crystal NR3	d_{220}(NR3)
d_{220} of Si crystal N	d_{220}(N)
d_{220} of Si crystal WASO 4.2a	d_{220}(W4.2a)
d_{220} of Si crystal WASO 04	d_{220}(W04)
d_{220} of an ideal Si crystal	d_{220}
d_{220} of Si crystal NR4	d_{220}(NR4)
Molar gas constant	R
Static electric dipole polarizability of ^{4}He in atomic units	$\alpha^*_0(^4He)$
Copper Kα_1 x unit	xu(CuKα_1
Ångstrom star	Å*
Molybdenum Kα_1 x unit	xu(MoKα_1

The electron–proton and electron-deuteron scattering values of the proton and deuteron rms radii, items *B*49 and *B*50, are the same as used in CODATA-14. Because the values of h, e, k, and N_A resulting from the CODATA 2017 Special Adjustment are essentially independent of r_p and r_d, the values chosen are not critical. This is shown in section 5.1, which discusses the result of using values for these radii obtained from measurements of the Lamb shift in muonic hydrogen and muonic deuterium.

3.3. Data that determine constants other than R_∞

Table 4 gives the principal input data that determine the 2017 Special Adjustment values of constants other than R_∞ and table 5 gives their correlation coefficients. Many of the data in table 4 are the same as (or fully equivalent to) those in the corresponding table XVIII of CODATA-14. The adjusted constants in terms of which the input data in table 4 are expressed are given in table 6 and their observational equations are given in table 7. As for the Rydberg constant data, the discussion of these data follows the order in which they are listed in table 4.

3.3.1. Atomic masses and binding energies. The relative atomic masses of the neutron n, ^{1}H, ^{2}H (deuterium, D), ^{3}H (tritium, T), ^{3}He, ^{4}He, ^{28}Si, and ^{87}Rb, which are data items *B*1, *B*2, *B*4, *B*6, *B*8, *B*10, *B*18, and *B*40 in table 4, are from AME2016, the most recent atomic mass evaluation from the AMDC, Lanzhou (Huang *et al* 2017, Wang *et al* 2017). AME2016 supersedes AME2012 used in CODATA-14. Since the results from the University of Washington and the Florida State University included in the 2014 adjustment as separate input data have been taken into account in AME2016, they no longer are treated separately and the values of $A_r(^2H)$, $A_r(^3H)$, and $A_r(^3He)$ from AME2016 are used. The values above are also listed in table 8 together with those for ^{36}Ar, ^{38}Ar, and ^{40}Ar. However, the argon values are not actual input data but are employed in the calculation of the molar mass of a particular argon sample used in the NIST, Gaithersburg, 1988 acoustic gas thermometry measurement of the molar gas constant R.

Extra digits were supplied to the Task Group by Task Group and AMDC member M. Wang to reduce rounding error. The covariances among the eight AME2016 values in table 8 used as input data are taken from the supplementary files at the AMDC website http://amdc.impcas.ac.cn/web/masseval.html and are used as appropriate in calculations; they are given in the form of correlation coefficients in table 5. However, the correlation coefficients for the argon relative atomic masses are negligible in the context in which the masses are used and are not included in the table.

Observational equations *B*1 and *B*40 in table 8 for input data $A_r(n)$ and $A_r(^{87}Rb)$ are quite simple. However, observational equations *B*2, *B*4, *B*6, *B*8, *B*10, and *B*18 for the other relative atomic masses are not because their purpose is to provide values of the relative atomic masses of the proton p, deuteron d, triton t, helion h (nucleus of ^{3}He), alpha particle (nucleus of ^{4}He), and hydrogenic ^{28}Si, respectively. Similarly, the denominator on the right-hand-side of observational equation *B*12 and the term in square brackets on the right-hand-side of *B*14 determine the relative atomic mass of the ^{12}C nucleus and of hydrogenic ^{12}C, respectively. These equations follow from the fact that to produce an ion X^{n+} with net charge ne, the energy required to remove n electrons from the neutral atom is the sum of the electron ionization energies $E_I(X^{i+})$. Thus, the relative atomic mass of an atom, its ions, the relative atomic mass of the electron $A_r(e)$, and the relative-atomic-mass equivalent of the binding energy of the removed electrons $E_B(X^{n+})/m_uc^2$ are related according to

Table 7. Observational equations that express the input data in table 4 as functions of the adjusted constants in table 6. The numbers in the first column correspond to the numbers in the first column of table 4. For simplicity, the lengthier functions are not explicitly given. See section 3.2 for an explanation of the symbol $\doteq$.

Type of input datum	Observational equation
*B*1	$A_r(\mathrm{n}) \doteq A_r(\mathrm{n})$
*B*2	$A_r(^1\mathrm{H}) \doteq A_r(\mathrm{p}) + A_r(\mathrm{e}) - \Delta E_B(^1\mathrm{H}^+)\,\alpha^2 A_r(\mathrm{e})/2R_\infty hc$
*B*3	$\Delta E_B(^1\mathrm{H}^+)/hc \doteq \Delta E_B(^1\mathrm{H}^+)/hc$
*B*4	$A_r(^2\mathrm{H}) \doteq A_r(\mathrm{d}) + A_r(\mathrm{e}) - \Delta E_B(^2\mathrm{H}^+)\,\alpha^2 A_r(\mathrm{e})/2R_\infty hc$
*B*5	$\Delta E_B(^2\mathrm{H}^+)/hc \doteq \Delta E_B(^2\mathrm{H}^+)/hc$
*B*6	$A_r(^3\mathrm{H}) \doteq A_r(\mathrm{t}) + A_r(\mathrm{e}) - \Delta E_B(^3\mathrm{H}^+)\,\alpha^2 A_r(\mathrm{e})/2R_\infty hc$
*B*7	$\Delta E_B(^3\mathrm{H}^+)/hc \doteq \Delta E_B(^3\mathrm{H}^+)/hc$
*B*8	$A_r(^3\mathrm{He}) \doteq A_r(\mathrm{h}) + 2\mathrm{A_r(e)} - \Delta E_B(^3\mathrm{He}^{2+})\,\alpha^2 \mathrm{A_r(e)}/2\mathrm{R}_\infty \mathrm{hc}$
*B*9	$\Delta E_B(^3\mathrm{He}^{2+})/hc \doteq \Delta E_B(^3\mathrm{He}^{2+})/hc$
*B*10	$A_r(^4\mathrm{He}) \doteq A_r(\alpha) + 2A_r(\mathrm{e}) - \Delta E_B(^4\mathrm{He}^{2+})\,\alpha^2 A_r(\mathrm{e})/2R_\infty hc$
*B*11	$\Delta E_B(^4\mathrm{He}^{2+})/hc \doteq \Delta E_B(^4\mathrm{He}^{2+})/hc$
*B*12	$\dfrac{\omega_c(^{12}\mathrm{C}^{6+})}{\omega_c(\mathrm{p})} \doteq \dfrac{6A_r(\mathrm{p})}{12 - 6A_r(\mathrm{e}) + \Delta E_B(^{12}\mathrm{C}^{6+})\,\alpha^2 A_r(\mathrm{e})/2R_\infty hc}$
*B*13	$\Delta E_B(^{12}\mathrm{C}^{6+})/hc \doteq \Delta E_B(^{12}\mathrm{C}^{6+})/hc$
*B*14	$\dfrac{\omega_s\left(^{12}\mathrm{C}^{5+}\right)}{\omega_c\left(^{12}\mathrm{C}^{5+}\right)} \doteq -\dfrac{g_C(\alpha) + \delta_C}{10A_r(\mathrm{e})}\left[12 - 5A_r(\mathrm{e}) + \Delta E_B\left(^{12}\mathrm{C}^{5+}\right)\alpha^2 A_r(\mathrm{e})/2R_\infty hc\right]$
*B*15	$\Delta E_B(^{12}\mathrm{C}^{5+})/hc \doteq \Delta E_B(^{12}\mathrm{C}^{5+})/hc$
*B*16	$\delta_C \doteq \delta_C$
*B*17	$\dfrac{\omega_s\left(^{28}\mathrm{Si}^{13+}\right)}{\omega_c\left(^{28}\mathrm{Si}^{13+}\right)} \doteq -\dfrac{g_{Si}(\alpha) + \delta_{Si}}{26A_r(\mathrm{e})} A_r(^{28}\mathrm{Si}^{13+})$
*B*18	$A_r(^{28}\mathrm{Si}) \doteq A_r(^{28}\mathrm{Si}^{13+}) + 13A_r(\mathrm{e}) - \Delta E_B(^{28}\mathrm{Si}^{13+})\,\alpha^2 A_r(\mathrm{e})/2R_\infty hc$
*B*19	$\Delta E_B(^{28}\mathrm{Si}^{13+})/hc \doteq \Delta E_B(^{28}\mathrm{Si}^{13+})/hc$
*B*20	$\delta_{Si} \doteq \delta_{Si}$
*B*21	$a_e \doteq a_e(\alpha) + \delta_e$
*B*22	$\delta_e \doteq \delta_e$
*B*23	$\overline{R} \doteq -\dfrac{a_\mu}{1 + a_e(\alpha) + \delta_e}\dfrac{m_e}{m_\mu}\dfrac{\mu_e}{\mu_p}$
*B*24, *B*25	$\nu(f_p) \doteq \nu\left(f_p; R_\infty, \alpha, \dfrac{m_e}{m_\mu}, a_\mu, \dfrac{\mu_e}{\mu_p}, \delta_e, \delta_{Mu}\right)$
*B*26	$\Delta\nu_{Mu} \doteq \Delta\nu_{Mu}\left(R_\infty, \alpha, \dfrac{m_e}{m_\mu}, a_\mu\right) + \delta_{Mu}$
*B*27	$\delta_{Mu} \doteq \delta_{Mu}$
*B*28	$\dfrac{\mu_p}{\mu_N} \doteq -(1 + a_e(\alpha) + \delta_e)\dfrac{A_r(\mathrm{p})}{A_r(\mathrm{e})}\dfrac{\mu_p}{\mu_e}$
*B*29	$\dfrac{\mu_e(\mathrm{H})}{\mu_p(\mathrm{H})} \doteq \dfrac{g_e(\mathrm{H})}{g_e}\left(\dfrac{g_p(\mathrm{H})}{g_p}\right)^{-1}\dfrac{\mu_e}{\mu_p}$
*B*30	$\dfrac{\mu_d(\mathrm{D})}{\mu_e(\mathrm{D})} \doteq \dfrac{g_d(\mathrm{D})}{g_d}\left(\dfrac{g_e(\mathrm{D})}{g_e}\right)^{-1}\dfrac{\mu_d}{\mu_e}$
*B*31	$\dfrac{\mu_e(\mathrm{H})}{\mu'_p} \doteq \dfrac{g_e(\mathrm{H})}{g_e}\dfrac{\mu_e}{\mu'_p}$
*B*32	$\dfrac{\mu'_h}{\mu'_p} \doteq \dfrac{\mu'_h}{\mu'_p}$
*B*33	$\dfrac{\mu_n}{\mu'_p} \doteq \dfrac{\mu_n}{\mu'_p}$
*B*34	$\dfrac{\mu_p(\mathrm{HD})}{\mu_d(\mathrm{HD})} \doteq [1 + \sigma_{dp}]\dfrac{\mu_p}{\mu_e}\dfrac{\mu_e}{\mu_d}$
*B*35	$\dfrac{\mu_t(\mathrm{HT})}{\mu_p(\mathrm{HT})} \doteq [1 - \sigma_{tp}]\dfrac{\mu_t}{\mu_p}$
*B*36	$\sigma_{dp} \doteq \sigma_{dp}$

(*Continued*)

Table 7. (Continued)

Type of input datum	Observational equation
*B*37	$\sigma_{tp} \doteq \sigma_{tp}$
*B*38	$h \doteq h$
*B*39	$\frac{h}{m(^{87}\mathrm{Rb})} \doteq \frac{A_r(e)}{A_r(^{87}\mathrm{Rb})}\frac{c\alpha^2}{2R_\infty}$
*B*40	$A_r(^{87}\mathrm{Rb}) \doteq A_r(^{87}\mathrm{Rb})$
*B*41-*B*50	$\frac{d_{220}(X)}{d_{220}(Y)} - 1 \doteq \frac{d_{220}(X)}{d_{220}(Y)} - 1$
*B*51-*B*53	$d_{220}(X) \doteq d_{220}(X)$
*B*54	$N_A \doteq \frac{cM_uA_r(e)\alpha^2}{2R_\infty h}$
*B*55	$R \doteq R$
*B*56	$\frac{k}{h} \doteq \frac{2R_\infty R}{cM_uA_r(e)\alpha^2}$
*B*57	$\frac{A_\epsilon(^4\mathrm{He})}{R} \doteq \frac{\alpha_0(^4\mathrm{He})}{4\pi\epsilon_0 a_0^3}\frac{cM_uA_r(e)\alpha^5}{96\pi^2 RhR_\infty^4}$
*B*58	$\frac{\alpha_0(^4\mathrm{He})}{4\pi\epsilon_0 a_0^3} \doteq \frac{\alpha_0(^4\mathrm{He})}{4\pi\epsilon_0 a_0^3}$
*B*59, *B*60	$\frac{\lambda(\mathrm{CuK}\alpha_1)}{d_{220}(X)} \doteq \frac{1\,537.400\ \mathrm{xu}(\mathrm{CuK}\alpha_1)}{d_{220}(X)}$
*B*61	$\frac{\lambda(\mathrm{WK}\alpha_1)}{d_{220}(\mathrm{N})} \doteq \frac{0.209\,010\,0\ \text{Å}^*}{d_{220}(\mathrm{N})}$
*B*62	$\frac{\lambda(\mathrm{MoK}\alpha_1)}{d_{220}(\mathrm{N})} \doteq \frac{707.831\ \mathrm{xu}(\mathrm{MoK}\alpha_1)}{d_{220}(\mathrm{N})}$

Table 8. Relative atomic masses used in the CODATA 2017 Special Adjustment as given in the 2016 atomic mass evaluation and the defined value for ^{12}C.

Atom	Relative atomic mass $A_r(X)$	Relative standard uncertainty u_r
n	1.008 664 915 82(49)	4.9×10^{-10}
^{1}H	1.007 825 032 241(94)	9.3×10^{-11}
^{2}H	2.014 101 778 11(12)	6.0×10^{-11}
^{3}H	3.016 049 281 98(23)	7.7×10^{-11}
^{3}He	3.016 029 322 65(22)	7.3×10^{-11}
^{4}He	4.002 603 254 130(63)	1.6×10^{-11}
^{12}C	12	(exact)
^{28}Si	27.976 926 534 99(52)	1.9×10^{-11}
^{36}Ar	35.967 545 105(29)	8.1×10^{-10}
^{38}Ar	37.962 732 10(21)	5.5×10^{-9}
^{40}Ar	39.962 383 1238(24)	6.0×10^{-11}
^{87}Rb	86.909 180 5312(65)	7.4×10^{-11}

$$A_r(X) = A_r(X^{n+}) + nA_r(e) - \frac{\Delta E_B(X^{n+})}{m_u c^2}, \qquad (1)$$

where

$$\frac{\Delta E_B(X^{n+})}{m_u c^2} = \frac{\alpha^2 A_r(e)}{2R_\infty}\frac{\Delta E_B(X^{n+})}{hc}, \qquad (2)$$

and where $m_u = m(^{12}\mathrm{C})/12$ is the atomic mass constant and α is the fine-structure constant. Equation (2) accounts for the fact that the binding energies are known most accurately in terms of their wavenumber equivalents and follows from the relations $m_e = A_r(e)m_u$ and $R_\infty = \alpha^2 m_e c/2h$.

All eight removal energies used in the 2017 Special Adjustment, items *B*3, *B*5, *B*7, *B*9, *B*11, *B*13, *B*15, and *B*19 in table 4, are obtained from the ionization energies given in the current version of the NIST online Atomic Spectra Database (Kramida *et al* 2017). The only change since 2014 is that for the ionization energy $^{12}C^{3+}$; the last digit is now 3 rather than 8 (see table III in CODATA-14). However, the correlation coefficient of the $^{12}C^{6+}$ and $^{12}C^{5+}$ removal energies is unchanged from its CODATA-14 value 1.000 and is included in table 5.

Item *B*12 in table 4 with identification MPIK-17, the ratio of the cyclotron frequency of the $^{12}C^{6+}$ ion to that of the proton in the same magnetic flux density B, is a new result obtained at MPIK, Heidelberg, and reported by Heiße *et al* (2017). Its observational equation, *B*12 in table 7, shows that, like input datum *B*2 with observational equation *B*2, the frequency ratio $\omega_c(^{12}C^{6+})/\omega_c(p)$ determines $A_r(p)$.

The MPIK-17 datum was obtained using a cryogenic Penning trap optimized for mass measurements of light ions. It has a measurement trap on either side of which is a storage trap. A proton stored in one and a $^{12}C^{6+}$ ion in the other are alternately shuttled back and forth into the measurement trap where its cyclotron frequency is determined. In parts in 10^{11}, the statistical relative standard uncertainty of the measured frequency ratio is 1.52 and the net correction for various systematic effects is 3.82 with an uncertainty of 2.89. The largest contributor to the latter uncertainty is 2.75 due to an effect

termed residual magnetostatic inhomogeneity and the largest correction, 9.10, is for image charge.

As discussed in section 4, the uncertainty of $A_r(p)$ obtained from $\omega_c(^{12}C^{6+})/\omega_c(p)$ is about 1/3 that of $A_r(p)$ obtained from $A_r(^1H)$ of AME2016, but the two values disagree. The MPIK researchers were aware of this and performed measurements on other ions that confirmed literature values; they were unable to identify any systematic effects in their method that would explain the inconsistency.

3.3.2. Hydrogenic carbon and silicon g-factors. Data item *B*14 in table 4 is the ratio of the spin-precession (spin-flip) frequency of the $^{12}C^{5+}$ hydrogenic ion to its cyclotron frequency in the same applied magnetic flux density *B*; and data item *B*17 is the similar ratio for the hydrogenic ion $^{28}Si^{13+}$. They are correlated with a correlation coefficient of 0.347, and the experiments on which they are based are discussed in CODATA-14. These ratios, which were obtained at MPIK, Heidelberg, together with the theory of the electron bound-state *g*-factor in the C and Si hydrogenic ions, provide a value for the electron relative atomic mass $A_r(e)$ with u_r of a few parts in 10^{11}.

The observational equations for the $^{12}C^{5+}$ and $^{28}Si^{13+}$ frequency ratios are *B*14 and *B*17 in table 7. In those equations $g_C(\alpha) + \delta_C$ and $g_{Si}(\alpha) + \delta_{Si}$ represent the theoretical expressions of the bound-state *g*-factors $g(^{12}C^{5+})$ and $g(^{28}Si^{13+})$. The theory of these *g*-factors is discussed in CODATA-14 and the only changes are as follows: (i) the remainder terms $R_{SE}(6\alpha) = 22.160(10)$ and $R_{SE}(14\alpha) = 20.999(2)$, which are equations (155) and (156) in CODATA-14, are replaced by the improved values $R_{SE}(6\alpha) = 22.166(1)$ and $R_{SE}(14\alpha) = 21.0005(1)$ obtained by Yerokhin and Harman (2017); and (ii) an additional term from light-by-light scattering diagrams calculated by Czarnecki and Szafron (2016) has been included in equation (164) of CODATA-14 for the $C_e^{(4)}(Z\alpha)$ coefficient. This contribution is similar to that discussed in section 3.2 in connection with the changes in the H and D energy level theory

The uncertainties of the additive corrections to the carbon and silicon theory, δ_C and δ_{Si}, items *B*7 and *B*11 in table 4, are nearly the same as their CODATA-14 values as is their covariance and hence correlation coefficient; these are now $u(\delta_C, \delta_{Si}) = 3.4 \times 10^{-20}$ and $r(\delta_C, \delta_{Si}) = 0.71$. The observational equations for the carbon and silicon additive corrections, *B*7 and *B*11 in table 7, are simply $\delta_C \doteq \delta_C$ and $\delta_{Si} \doteq \delta_{Si}$.

It is worth noting that the value of $A_r(e)$ recently obtained by Zatorski *et al* (2017) from their treatment of the MPIK frequency ratios and review of the *g*-factor theory and the value resulting from our treatment are essentially identical.

3.3.3. Electron and muon magnetic moment anomalies. The most accurate value of α is obtained by equating the experimental value of the electron magnetic moment anomaly a_e and its theoretical expression. Item *B*21 in table 4 with $u_r = 2.4 \times 10^{-10}$ is the experimental value of a_e with the smallest uncertainty achieved to date. Discussed in CODATA-10 and used in both the 2010 and 2014 adjustments, it was obtained at Harvard University, Cambridge, using a Penning trap (Hanneke *et al* 2008); no other result is competitive.

As discussed in CODATA-14, the theoretical expression for a_e can be written as

$$a_e(\text{th}) = a_e(\text{QED}) + a_e(\text{weak}) + a_e(\text{had}). \tag{3}$$

The electroweak and hadronic contributions are small compared with the quantum electrodynamic contribution a_e(QED). The latter is currently written as the sum of five terms of the form $C_e^{(2n)}(\alpha/\pi)^n$ with $n = 1, 2, 3, 4$, and 5, since terms for $n > 5$ are assumed to be negligible at the level of uncertainty of a_e(exp). Various terms dependent on the mass ratios m_e/m_μ and m_e/m_τ contribute to the coefficients $C_e^{(2n)}$ except for $n = 1$. Following CODATA-14 and using the 2017 adjusted values of these mass ratios, the five coefficients are

$$\begin{aligned} C_e^{(2)} &= 0.5, \\ C_e^{(4)} &= -0.328\,478\,444\,00\ldots, \\ C_e^{(6)} &= 1.181\,234\,017\ldots, \\ C_e^{(8)} &= -1.911\,322\,138\,91(88), \\ C_e^{(10)} &= 6.60(22), \end{aligned} \tag{4}$$

where two new results have been incorporated in $C_e^{(8)}$ and $C_e^{(10)}$. First, in the mass-independent contribution to a_e(QED), the numerically calculated eighth-order coefficient used in CODATA-14 due to Aoyama *et al* (2015), $A_1^{(8)} = -1.912\,98(84)$, is replaced with the semi-analytical value $A_1^{(8)} = -1.912\,245\,764\ldots$ obtained by Laporta (2017). This coefficient depends on 891 4-loop Feynman diagrams and its evaluation is difficult; Laporta's result with 1100 digit accuracy is the culmination of a 20-year effort. It is noteworthy that the numerically calculated result differs from its essentially exact counterpart by less than 0.9σ.

Second, and again in the mass-independent contribution to a_e(QED), the numerically calculated tenth-order coefficient employed in CODATA-14, $A_1^{(10)} = 7.795(336)$, also due to Aoyama *et al* (2015), is replaced with $A_1^{(10)} = 6.599(223)$. This newly revised result published as an erratum (Aoyama *et al* 2017) is a consequence of their correction of an error discovered in a portion of their previous calculation and additional numerical evaluations. The coefficient $A_1^{(10)}$ depends on 12 672 Feynman diagrams and its determination is formidable.

The sum of a_e(weak) given in CODATA-14 and the values of the various corrections that contribute to a_e(had) also given there is $1.735(15) \times 10^{-12}$ and is the value used in the 2017 Special Adjustment. It is consistent with the value $1.723(11) \times 10^{-12}$ obtained by Jegerlehner (2017) based on his own independent evaluation of each contribution and employing up-to-date experimental data.

The uncertainties of the coefficients $C_e^{(8)}$ and $C_e^{(10)}$ together with those of the weak and hadronic contributions yield for the standard uncertainty of the theoretical value $u[a_e(\text{th})] = 0.021 \times 10^{-12}$. The theoretical expression for a_e is written as $a_e(\text{th}) = a_e(\alpha) + \delta_e$, where the additive correction δ_e is equal to $0.000(21) \times 10^{-12}$ and is input datum *B*22 in table 4. The observational equation for a_e is *B*21 in table 7 and the observational equation for the additive correction is simply $\delta_e \doteq \delta_e$, which is equation *B*22 in table 7. The value of

Table 9. Inferred values of the fine-structure constant α in order of increasing standard uncertainty obtained from the indicated experimental data in table 4.

Primary source	Item number	Identification	α^{-1}	Relative standard uncertainty u_r
a_e	*B*21	HarvU-08	137.035 999 150(33)	2.4×10^{-10}
$h/m(^{87}\mathrm{Rb})$	*B*39	LKB-11	137.035 998 995(85)	6.2×10^{-10}

α that results from equating the Harvard experimental value and $a_e(\mathrm{th})$ is given in table 9.

The muon magnetic moment anomaly a_μ is required to obtain m_e/m_μ from measurements involving muonium (see next section). As discussed in CODATA-14, the experimental value of a_μ is derived from the BNL, Upton, measurement of the quantity $\bar{R} = f_a/\bar{f}_p$, which is item *B*23 in table 4. Here f_a is the anomaly difference frequency equal to the difference between the muon spin-flip (precession) frequency and cyclotron frequency in the same applied magnetic flux density B, and $\bar{f}_p$ is the free proton nuclear magnetic resonance (NMR) frequency corresponding to the average B seen by the circulating muons in their storage ring. The observational equation *B*23 in table 7 for the input datum $\bar{R}$ shows its relationship with the adjusted constants a_μ and m_e/m_μ as well as others.

The theoretical expression for a_μ is omitted from both CODATA-10 and 14 because of concerns regarding the theory. Inasmuch as these concerns remain, the theory is also omitted from the 2017 Special Adjustment. However, its omission has no effect on the chosen numerical values of h, e, k, and N_A.

3.3.4. Muonium hyperfine splitting. Determination of the ground-state hyperfine-splitting of muonium (μ^+e atom) together with the theory of the splitting determines m_e/m_μ, which in turn enters the theory of the electron and muon magnetic moment anomalies. The available experimental data are from two experiments carried out at LAMPF, Los Alamos, and reported in 1982 and 1999.

In these experiments two Zeeman transition frequencies are measured with the muonium atoms in an applied magnetic flux density B known in terms of a free proton NMR frequency f_p. The sum of the two frequencies is the hyperfine splitting frequency $\Delta\nu_{Mu}$ and their difference is a frequency denoted $\nu(f_p)$. The experiments are discussed in CODATA-98 and there have been no changes in the data since then. The two 1982 and two 1999 frequencies are items *B*24 and *B*26.1, and *B*25 and *B*26.2, in table 4. Their observational equations are *B*24, *B*25 and *B*26 in table 7. For each experiment the two frequencies are correlated; the correlation coefficients are $r[\Delta\nu_{Mu}, \nu(f_p)] = 0.227$ for the 1982 data and $r[\Delta\nu_{Mu}, \nu(f_p)] = 0.195$ for the 1999 data and are taken into account in calculations. For the 1982 data $f_p = 57.972\,993$ MHz corresponding to B of about 1.4 T and for the 1999 data $f_p = 72.320\,000$ MHz corresponding to B of about = 1.7 T.

There has been no change in the theory since the 31 December 2014 closing date of CODATA-14, hence the uncertainty $u(\delta_{Mu}) = 85$ Hz of the additive correction δ_{Mu} used in the 2014 adjustment to account for the uncertainty of the theory is unchanged. The correction δ_{Mu} is item *B*27 in table 4 and its observational equation is simply $\delta_{Mu} \doteq \delta_{Mu}$, which is equation *B*27 in table 7.

3.3.5. Magnetic moment ratios. Discussed in this section are the six input data *B*28-*B*35 in table 4 with observational equations *B*28-*B*35 in table 7. Some of these data contribute to the determination of the adjusted constant μ_e/μ_p, which in turn contributes to the determination of the adjusted constant m_e/m_μ. The latter is required for the theoretical expression of a_e and a_μ. In item *B*28, $\mu_N = e\hbar/2m_p$ is the nuclear magneton, and in items *B*29-*B*31 and *B*34.1 - *B*35, $\mu_X(Y)$ is the magnetic moment of particle X in atom or molecule Y. These data have been discussed in earlier CODATA reports and all are used in CODATA-14. The exception is input data *B*36 and *B*37 for adjusted constants $\sigma_{dp} = \sigma_d(\mathrm{HD}) - \sigma_p(\mathrm{HD})$ and $\sigma_{tp} = \sigma_t(\mathrm{HT}) - \sigma_p(\mathrm{HT})$, the differences between the magnetic shielding correction of the deuteron and of the proton in the HD molecule and of the triton and of the proton in the HT molecule. They are the improved theoretical values reported by Puchalski *et al* (2015) and although discussed in CODATA-14, they were not included in the 2014 adjustment because they became available only after its 31 December 2014 closing date.

The observational equations in table 7 for items *B*29 to *B*31 contain four bound-particle to free particle ratios of the form $g_X(Y)/g_X$, where X is either e, p, or d, and Y is either H or D. These ratios are calculated theoretically and have sufficiently small uncertainties in the context in which they are used to be taken as exact. Their values have not changed since CODATA-02 and are given in table XIII of CODATA-14.

3.3.6. Kibble and joule balance measurements of h. The watt balance was conceived by Bryan Kibble of NPL, Teddington, in 1975. With the discovery of the quantum-Hall effect in 1980 it became a means of measuring h. Upon the passing of Kibble in April 2016 the Consultative Committee for Units (CCU) of the CIPM decided to honor him by renaming the 'watt balance' the 'Kibble balance' and this is the name used herein (CCU 2016).

How the Kibble balance determines h is discussed in CODATA-98, and values of h so obtained have been included in all CODATA adjustments ever since. The five values considered for inclusion in the CODATA 2017 Special Adjustment are items *B*38.1-*B*38.5 in table 4.

The NIST-98 value of h, item *B*38.1, was obtained by Williams *et al* (1998) using a Kibble balance called NIST-2 that operated in air and used a superconducting magnet to generate the required magnetic flux density B; it is discussed in CODATA-98, but see also CODATA-06. NIST-2 was replaced by a new Kibble balance called NIST-3 that operated

in vacuum but used the same superconducting magnet. The value of h obtained from this apparatus with $u_r = 3.6 \times 10^{-8}$, identified as NIST-07, was taken as an input datum in both the 2006 and 2010 adjustments. However, as discussed in CODATA-14, issues with the NIST-07 result were uncovered that led to a number of improvements in the NIST-3 apparatus, additional data, and a thorough review of all previous NIST-3 data. This led to the value identified as NIST-15, item *B*38.2 in table 4. As reported by Schlamminger *et al* (2015), it is viewed as the final result from NIST-3 and is used as an input datum in CODATA-14. The NIST-98 and NIST-15 values are correlated with a correlation coefficient of 0.09.

NIST-3 was replaced by a completely new Kibble balance called NIST-4. It uses a permanent magnet rather than a superconducting magnet to generate B but as in NIST-2 and NIST-3, a wheel is used as the balance beam and to displace the moving coil. Haddad *et al* (2016) discuss the new apparatus, measurement procedures, and sources of uncertainty and report a first result with $u_r = 3.4 \times 10^{-8}$ based on data obtained from mid-December 2015 to early January 2016 using a 1 kg 90% Pt-10% Ir mass standard. After obtaining this first result the NIST researchers continued improving NIST-4 and acquiring additional data. Based on all 1174 individual determinations of h obtained from mid-December 2015 through April 2017, Haddad *et al* (2017) report the result identified as NIST-17, item *B*38.3 in table 4, with $u_r = 1.3 \times 10^{-8}$. Each measurement was carried out with one of five different 0.5 kg stainless steel mass standards, a 1 kg stainless steel standard, or one of two 1 kg Pt-Ir standards, and various combinations to provide standards in the range 0.5 kg to 2 kg.

The uncertainty of the initial NIST-4 result was reduced by more than a factor of 2.5 by (i) making significantly more measurements of h, thus allowing a more realistic statistical analysis of the data; (ii) using mass standards as large as 2 kg to more thoroughly investigate the effect of the current in the moving coil on the magnet generating the magnetic flux density B; and (iii) carefully investigating the effect of coil velocity on the measurements, thereby enabling reduction of the uncertainty due to time-dependent leakage of current in the coil. As a result of these advances, the 24.9 parts in 10^9 statistical uncertainty and 15.4 parts in 10^9 magnetic field uncertainty of the first result are reduced to 3.0 and 1.8 parts in 10^9, respectively. The main contributors to the uncertainty of the 2017 result are, in parts in 10^9, 6.2 for electrical, 6.1 for mass metrology, 5.0 for magnetic field profile fitting, 5.0 for balance mechanics, 4.7 for alignment, and 4.3 for the local gravitational acceleration.

Item *B*38.4 in table 4 from NRC, Ottawa, identified as NRC-17 and reported by Wood *et al* (2017), was obtained using the NRC Kibble balance. The history of this balance, which was originally the NPL, Teddington, Mark II balance but was transferred to NRC in the summer of 2009, is discussed in CODATA-14. That discussion covers the measurements made with it prior to its transfer, the many significant improvements made to it at NRC, and the result identified as NRC-14 with $u_r = 1.8 \times 10^{-8}$ used as an input datum in CODATA-14. This value was based on four measurement campaigns carried out between September and December 2013 using four different mass standards.

The new NRC-17 result is based on a reanalysis of the 2013 measurements and three new determinations carried out in February, November, and December 2016 with the same 500 g silicon, 1 kg AuCu, and 500 g AuCu mass standards used in 2013. However, additional improvements were made to the apparatus between the 2013 and 2016 campaigns. The reported final result, which has the smallest uncertainty of any value of h available to date, was obtained by combining all seven values from the seven measurement campaigns taking into account the covariances among them from the 58 uncertainty components that contribute to the uncertainty of each value. The procedure used is the same as used by the Task Group to carry out least-squares adjustments as discussed in appendix E of CODATA-98. A previously unidentified systematic effect, the hysteresis of the magnetization of the permanent magnet used to generate B due to the current in the required moving coil of a Kibble balance, was quantified and a correction that averaged 3.8 parts in 10^9 was applied to each of the seven values. The total uncertainty is not dominated by any one component.

Item *B*38.5, reported by Thomas *et al* (2017) and identified as LNE-17, is the most recent and accurate result from the LNE, Trappes, Kibble-balance project initiated in 2001. A first result reported by Thomas *et al* (2015) with $u_r = 3.1 \times 10^{-7}$ was obtained in 2014 and an improved result with $u_r = 1.4 \times 10^{-7}$ in 2016 in the course of the BIPM's Extraordinary Calibration Campaign. Improvements in the apparatus and measurement procedures continued, including better calibration of the 500 g pure iridium mass standard used in the experiment's weighing phase, reduction of the Type A (statistical) uncertainty, better alignment of the balance's various laser beams, and use of a programmable Josephson effect voltage standard. The LNE-17 result was obtained over a 35 d period during the spring of 2017.

An important feature of the LNE Kibble balance is that instead of having the beam of the balance used in the weighing phase also move the coil in the dynamic phase, the entire balance and suspended coil are moved by a translation stage. In contrast to the NIST and NRC Kibble balances that are operated in vacuum, to date the LNE balance has only been operated in air. The 4.7 parts in 10^8 uncertainty of the required correction for the refractive index of air and air buoyancy is the dominant contributor to the 5.7 parts in 10^8 total uncertainty.

Li *et al* (2017) have reported a first result for h from the NIM, Beijing, joule balance NIM-2 with $u_r = 2.4 \times 10^{-7}$ and in agreement with other values of h. The joule balance measures h in a manner similar to the Kibble balance but compares electric energy with gravitational potential energy rather than electric power with mechanical power. However, u_r of the result is too large for it to be considered for inclusion in the 2017 Special Adjustment, inasmuch as values of h with smaller u_r were not sufficiently competitive to be included in the final adjustment on which the CODATA 2014 recommended values are based.

Although the results for the five Kibble-balance results discussed above are given as values of h in table 4, in previous adjustments such results were given as values of $K_J^2 R_K = 4/h$ to facilitate tests of the exactness of the Josephson and quantum-Hall effect relations $K_J = 2e/h$ and $R_K = h/e^2$.

Table 10. Inferred values of the Planck constant h in order of increasing standard uncertainty obtained from the indicated experimental data in table 4.

Primary source	Item number	Identification	$h/(\mathrm{J\ s})$	Relative standard uncertainty u_r
h	$B38.4$	NRC-17	$6.626\,070\,133(60) \times 10^{-34}$	9.1×10^{-9}
$N_\mathrm{A}(^{28}\mathrm{Si})$	$B54.3$	IAC-17	$6.626\,070\,405(77) \times 10^{-34}$	1.2×10^{-8}
h	$B38.3$	NIST-17	$6.626\,069\,934(88) \times 10^{-34}$	1.3×10^{-8}
$N_\mathrm{A}(^{28}\mathrm{Si})$	$B54.2$	IAC-15	$6.626\,070\,22(13) \times 10^{-34}$	2.0×10^{-8}
$N_\mathrm{A}(^{28}\mathrm{Si})$	$B54.4$	NMIJ-17	$6.626\,070\,13(16) \times 10^{-34}$	2.4×10^{-8}
$N_\mathrm{A}(^{28}\mathrm{Si})$	$B54.1$	IAC-11	$6.626\,069\,94(20) \times 10^{-34}$	3.0×10^{-8}
h	$B38.5$	LNE-17	$6.626\,070\,40(38) \times 10^{-34}$	5.7×10^{-8}
h	$B38.2$	NIST-15	$6.626\,069\,36(38) \times 10^{-34}$	5.7×10^{-8}
h	$B38.1$	NIST-98	$6.626\,068\,91(58) \times 10^{-34}$	8.7×10^{-8}

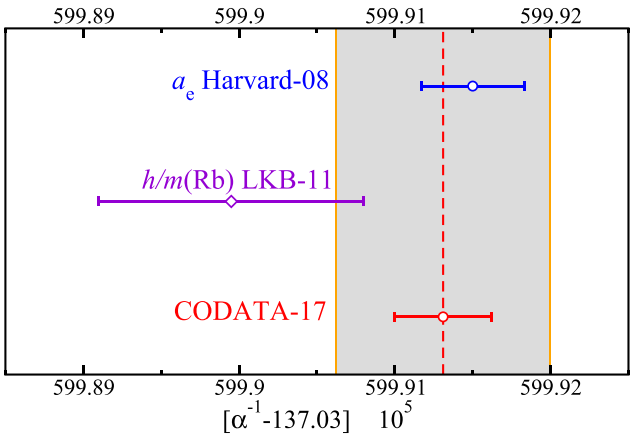

Figure 1. Comparison of input data $B21$ (HarvU-08) and $B39$ (LKB-11) through their inferred values of α (see table 9). Both $B21$ and $B39$ have the same value as in the 2010 and 2014 adjustments and are essentially the sole determinants of the recommended value of α in each. The grey band is ± 5 parts in 10^{10}.

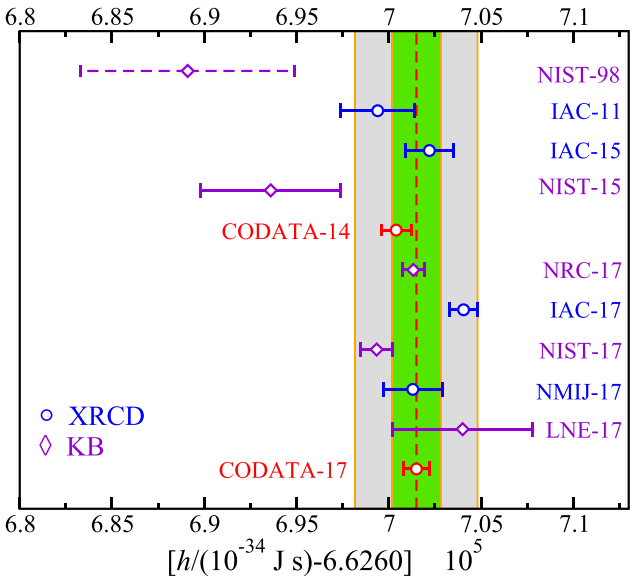

Figure 2. Values of the Planck constant h inferred from the input data in table 4, the CODATA 2014 value, and the CODATA 2017 value in chronological order from top to bottom (see table 10). Dashed values were not included in the final 2017 adjustment. The inner green band is ± 20 parts in 10^9 and the outer grey band is ± 50 parts in 10^9. KB: Kibble balance; XRCD: x-ray-crystal-density.

Further, the NIST, NRC, and LNE researchers have found it convenient to analyze their data and also to report their results as deviations from the conventional value of the Planck constant $h_{90} = 4/K_{\mathrm{J}-90}^2 R_{\mathrm{K}-90} = 6.626\,068\,854\ldots \times 10^{-34}$ J s, where $K_{\mathrm{J}-90}$ and $R_{\mathrm{K}-90}$ are the exact, conventional values of the Josephson and von Klitzing constants given in table 1. The reported values of $(h/h_{90}) - 1$ for the five results are, in parts in 10^9, 8(87), 77(57), 163(13), 193.0(9.1), and 234(57).

The five Kibble-balance values of h together with the four values of h that can be inferred from the four values of N_A discussed in section 3.3.9 are compared in table 10 and figure 2. The observational equation for Kibble-balance measurements of h is $B38$ in table 7 and is simply $h \doteq h$.

3.3.7. Measurement of h/m for ^{87}Rb. Accurate measurement of the quotient of h and the mass of a particle X can provide a competitive value of α through the equation

$$\alpha = \left[\frac{2R_\infty}{c}\frac{A_\mathrm{r}(X)}{A_\mathrm{r}(\mathrm{e})}\frac{h}{m(X)}\right]^{1/2}, \qquad (5)$$

where $A_\mathrm{r}(X)$ is the relative atomic mass of particle X with mass $m(X)$. This expression is a consequence of the definition of the Rydberg constant $R_\infty = \alpha^2 m_\mathrm{e} c/2h$.

Item $B39$ in table 4 is the value for $h/m(^{87}\mathrm{Rb})$ obtained at LKB, Paris, using Bloch oscillations together with atom interferometry. This result is discussed in CODATA-10 and its precursor in CODATA-06. Its observational equation is $B39$ in table 7 and follows directly from equation (5). The LKB result, with $u_\mathrm{r} = 1.2 \times 10^{-9}$ and which is used in both the 2010 and 2014 adjustments, provides a value of α with u_r about half as large because of the square root in equation (5) and because u_r of $A_\mathrm{r}(^{87}\mathrm{Rb})$, $A_\mathrm{r}(\mathrm{e})$, and R_∞ are at the parts in 10^{11} to parts in 10^{12} level. This value of α is given in table 9 together with that from a_e. These data are graphically compared in figure 1.

3.3.8. Natural silicon measurements. The data from measurements with naturally occurring silicon used in the 2017 Special Adjustment, which are discussed in this section, are identical to those employed in the 2014 adjustment; see section IX.A of CODATA-14.

In table 4, data $B41$-$B48$ and $B50$ are the directly measured fractional differences $[d_{220}(X) - d_{220}(\mathrm{ref})]/d_{220}(\mathrm{ref})$ between

the {220} crystal lattice spacing $d_{220}(X)$ of a nearly crystallographically perfect natural silicon crystal X and a similar reference crystal; $B49$ is the estimated difference between the {220} crystal lattice spacing of an ideal silicon crystal and that of crystal W04, both in vacuum and at a temperature of 22.5 °C; $B51$-$B53.2$ are the directly measured d_{220} values of the indicated crystals in vacuum and at 22.5 °C; and $B59$-$B62$ are the measured ratios of the wavelengths of the indicated x-ray lines to the {220} lattice spacing of the indicated crystal, also under the same conditions.

The observational equations for these data are $B41$-$B50$, $B51$-$B53$, $B59$, $B60$, $B61$, and $B62$ in table 7. The three conventional x-ray units $\mathrm{xu}(\mathrm{CuK}\alpha_1)$, Å^*, and $\mathrm{xu}(\mathrm{MoK}\alpha_1)$ in the last four observational equations are defined by assigning the indicated exact numerical value (the number in the numerator on the right-hand-side of each equation) to the $\mathrm{CuK}\alpha_1$, $\mathrm{WK}\alpha_1$, and $\mathrm{MoK}\alpha_1$ x-ray lines. Together, the 20 natural silicon x-ray data determine the {220} lattice spacing of each of the eight crystals involved in the measurements, d_{220} of an ideal silicon crystal, and the values of the three conventional x-ray units, all in meters.

3.3.9. Enriched silicon measurements of N_A. The x-ray-crystal-density (XRCD) method of measuring N_A is discussed in CODATA-98 and the progress made over the years is documented in subsequent CODATA reports. The International Avogadro Coordination (IAC) project to determine N_A with the smallest possible uncertainty was initiated in 2004. Consisting of a group of researchers working at several different institutions, the project has developed the XRCD method to the point where a relative uncertainty u_r approaching 1 part in 10^8 can be achieved.

Silicon in the form of highly polished, highly pure, nearly spherical, and nearly crystographically perfect spheres of nominal mass 1 kg composed of very nearly the single isotope ^{28}Si are the samples used in IAC work since about 2009. Required measurements include impurity content (point defects), isotopic composition, lattice spacing, sphere surface characterization (mass and thickness of contaminant layers), sphere mean diameter, and sphere mass. The techniques employed include isotope dilution mass spectrometry, combined x-ray and optical interferometry, optical interferometry, weighing with the highest possible accuracy, and for surface characterization x-ray fluorescence (XRF), x-ray reflectometry (XRR), optical spectral ellipsometry (SE), and x-ray photoelectron spectroscopy (XPS).

The four values of N_A in table 4, items $B54.1$ to 54.4, IAC-11, IAC-15, IAC-17, and NMIJ-17, are related. Their treatment in the 2017 Special Adjustment is based on a recommendation to the Task Group by the IAC (Fujii *et al* 2018) and is motivated by the way the IAC determined IAC-17 (Bartl *et al* 2017). In the latter experiment the {220} lattice spacing d_{220} was not directly measured but was derived from the mean of the d_{220} value obtained in the 2011 experiment and that obtained in the 2015 experiment. However, prior to the calculation of the mean, the IAC-11 value of d_{220} was corrected by the fractional amount 3.6×10^{-9} and the IAC-15 value by 2.9×10^{-9}. These corrections to the two d_{220} values are due to the discovery of a laser beam diffraction effect and a surface stress effect in the combined x-ray and optical interferometer (XROI) used to determine them. The diffraction effect is considered by Mana *et al* (2017) and also by Bartl *et al* (2017); the stress effect is considered in the latter paper and in the references cited therein. As we now discuss, this d_{220} 'consensus' mean value is used to correct the 2011 and 2015 IAC values of N_A as well as the 2017 NMIJ value of N_A, recognizing that the fractional change in N_A is -3 times the fractional change in d_{220}.

As reported by Andreas *et al* (2011) and reviewed in CODATA-10, item $B54.1$ in table 4 with identification IAC-11 is the first IAC enriched-silicon result. The two spheres used to obtain IAC-11 are denoted AVO28-S5 and AVO28-S8 and were manufactured from the ^{28}Si-enriched single crystal boule AVO28. As explained in CODATA-14, IAC-11 has been corrected by Azuma *et al* (2015) to account for the problem discovered at the BIPM, Sèvres, with the working standards BIPM was employing to disseminate the unit of mass. However, it now also includes a net fractional correction of -6.30×10^{-9} from two sources: (i) 3 times 0.10×10^{-9} due to the difference of the IAC-11 d_{220} value from the consensus value discussed above; and (ii) -6.61×10^{-9} due to the difference of the mean of the molar mass values obtained for the two AVO28 spheres used in the 2011 experiment from the more accurate and reliable molar mass value obtained in the 2015 experiment, which is the same for both spheres. Both IAC-15 and NMIJ-17 are based on this molar mass value and the IAC recommended that it be used to correct the 2011 N_A value (Fujii *et al* 2018).

Item $B54.2$, IAC-15, reported by Azuma *et al* (2015) and discussed in CODATA-14, was obtained after a number of improvements were incorporated in the initial XRCD experiment including re-etching and re-polishing the AVO28-S5 and AVO28-S8 spheres to remove metallic contaminants in the form of Cu, Ni, and Zn silicide compounds from their surfaces. The spheres were then re-labeled AVO28-S5c and AVO28-S8c. Also, the molar mass was obtained with a significantly reduced uncertainty based on measurements carried out in three different laboratories using improved chemistry. IAC-15 includes a correction of 3 times $-3.49 \times 10^{-9} = -10.47 \times 10^{-9}$ due to the difference of the IAC-15 d_{220} value from the consensus value discussed above.

Item $B54.3$, IAC-17, is a new result reported by Bartl *et al* (2017) in a detailed paper with many references. It was obtained using two new spheres called Si28kg01a and Si28kg01b manufactured at PTB, Braunschweig, from a new silicon single crystal boule labeled Si28-23Pr11. The ^{28}Si enrichment of the boule is 99.9985% compared with the 99.9956% enrichment of the AVO28 boule from which the AVO28-S5 and AVO28-S8 spheres were manufactured. The deviations of the spheres from perfect roundness are less than for the previous spheres and their surfaces show no detectable trace of metallic contaminants.

The crystal properties of the boule and their variations throughout its volume were carefully investigated using 27 samples from strategically selected locations. Measurements of point defects include amount of carbon, oxygen, boron, phosphorus, nitrogen, and vacancies. Measurements of the isotopic composition of the boule to determine the molar mass of the spheres were carried out on different samples bracketing the locations in the boule where the material used to

Table 11. Inferred values of the Boltzmann constant k in order of increasing standard uncertainty obtained from the indicated experimental data in table 4.

Primary source	Item number	Identification	$k/(\mathrm{J\ K^{-1}})$	Relative standard uncertainty u_r
R	$B55.9$	LNE-17	$1.380\,648\,80(83) \times 10^{-23}$	6.0×10^{-7}
R	$B55.8$	NPL-17	$1.380\,648\,62(96) \times 10^{-23}$	7.0×10^{-7}
R	$B55.5$	LNE-15	$1.380\,6487(14) \times 10^{-23}$	1.0×10^{-6}
R	$B55.6$	INRIM-15	$1.380\,6509(15) \times 10^{-23}$	1.1×10^{-6}
R	$B55.4$	LNE-11	$1.380\,6477(19) \times 10^{-23}$	1.4×10^{-6}
R	$B55.1$	NIST-88	$1.380\,6502(25) \times 10^{-23}$	1.8×10^{-6}
$A_e(^4\mathrm{He})/R$	$B57$	PTB-17	$1.380\,6482(27) \times 10^{-23}$	1.9×10^{-6}
R	$B55.7$	NIM-17	$1.380\,6484(28) \times 10^{-23}$	2.0×10^{-6}
k/h	$B56.2$	NIM/NIST-17	$1.380\,6497(37) \times 10^{-23}$	2.7×10^{-6}
R	$B55.2$	LNE-09	$1.380\,6497(38) \times 10^{-23}$	2.7×10^{-6}
R	$B55.3$	NPL-10	$1.380\,6498(44) \times 10^{-23}$	3.2×10^{-6}
k/h	$B56.1$	NIM/NIST-15	$1.380\,6516(53) \times 10^{-23}$	3.9×10^{-6}
k/h	$B56.3$	NIST-17	$1.380\,6430(69) \times 10^{-23}$	5.0×10^{-6}
R	$B55.10$	UVa/CEM-17	$1.380\,6467(93) \times 10^{-23}$	6.7×10^{-6}

manufacture the spheres was taken. This provided information about the possible variation of molar mass in the boule. The method used to determine the amount of substance fractions of the three silicon isotopes ^{28}Si, ^{29}Si, and ^{30}Si to determine molar mass was basically the same as used to obtain the result IAC-15. The mean diameter of each sphere and hence its volume was determined by optical interferometry and its mass by careful weighing in vacuum.

PTB researchers directly measured all but one of the necessary parameters to determine N_A using both spheres Si28kg01a and Si28kg01b, and researchers at NMIJ, Tsukuba, did the same for Si28kg01a. Although both laboratories devoted special effort to determining the properties of the contaminant surface layers on the spheres, PTB by XRR, XRF, and XPS, and NMIJ by XPS and SE, neither directly measured d_{220} of Si28-23Pr11 with an XROI. Rather, both obtained their value of d_{220} by independently deriving it from the consensus value discussed above. The PTB researchers did this by applying corrections for point defects and the difference in ^{28}Si enrichment of the AVO28 and Si28-23Pr11 boules. The NIMJ researchers did it by measuring the difference between an AVO28 sample and a Si28-23Pr11 sample using an instrument called a self-referenced lattice comparator and also applying corrections for point defects.

The relative uncertainty of the NMIJ value of N_A from sphere Si28kg01a is, in parts in 10^8, 2.3, and of the PTB values of N_A from spheres Si28kg01a and Si28kg01b, 1.4 and 1.4. The final result for N_A reported by Bartl *et al* (2017) is the weighted mean of the three values, which are in agreement, taking correlations into account. The IAC researchers are aware that their new result IAC-17 is not in as good agreement as they would like with their previous results IAC-11 and IAC-15 and with the new NMIJ-17 result discussed next, but to date have been unable to identify any cause.

The value of N_A identified as NMIJ-17, item $B54.4$ in table 4, was measured at NMIJ using sphere AVO28-S5c. Reported by Kuramoto *et al* (2017), the required parameters determined independently in this experiment are the mass of the sphere, obtained by comparison with a mass standard calibrated by the BIPM as part of the Extraordinary Calibration Campaign; the mean diameter of the sphere, obtained by optical interferometry; and the thickness and mass of its surface layers, obtained by XPS and SE. The other required parameters, molar mass, d_{220}, and mass of the point defects, are taken from the IAC-15 experiment (Azuma *et al* 2015). Thus, the NMIJ-17 value of N_A in table 4 includes the same -10.47×10^{-9} correction for d_{220} as does IAC-15. The main contributor to the total relative uncertainty of this result, $u_r = 2.4 \times 10^{-8}$, is the relative uncertainty of the NMIJ measured volume of the silicon core of the sphere, $u_r = 2.0 \times 10^{-8}$.

The inclusion of the correction for d_{220} and molar mass in the IAC-11 value of N_A, and the inclusion of the correction for d_{220} in the IAC-15 and NMIJ-17 values of N_A, requires a re-evalution of the six covariances among the four N_A values based on updated uncertainty budgets. These are given in table 5 in the form of correlation coefficients (Fujii *et al* 2018).

The observational equation for N_A is $B54$ in table 7 and follows from $R_\infty = \alpha^2 m_e c/2h$. This equation is noteworthy because it can be written as

$$h = \frac{cM_u A_r(e)\alpha^2}{2R_\infty N_A}. \tag{6}$$

Since c and the molar mass constant $M_u = 0.001\,\mathrm{kg\,mol^{-1}}$ are exact and u_r of the combination of constants $A_r(e)\alpha^2/R_\infty$ is 4.5×10^{-10}, a value of N_A with, say, $u_r = 2 \times 10^{-8}$ can provide a value of h with essentially the same uncertainty. Table 10 and figure 2 compare the values of h that can be so inferred from IAC-11, IAC-15, IAC-17, and NMIJ-17 with the Kibble balance values of h.

3.3.10. Thermal physical measurements that determine k. The 15 input data $B55$-$B58$ in table 4 determine 14 values of the Boltzmann constant k. These 14 inferred values are compared in table 11 and figure 3. The ten items $B55$ are acoustic gas thermometry (AGT) measurements of the molar gas constant $R = kN_A$. The three items $B56$ are Johnson noise thermometry (JNT) measurements of k/h. Finally, item $B57$ is a dielectric constant gas thermometry (DCGT) measurement of gaseous

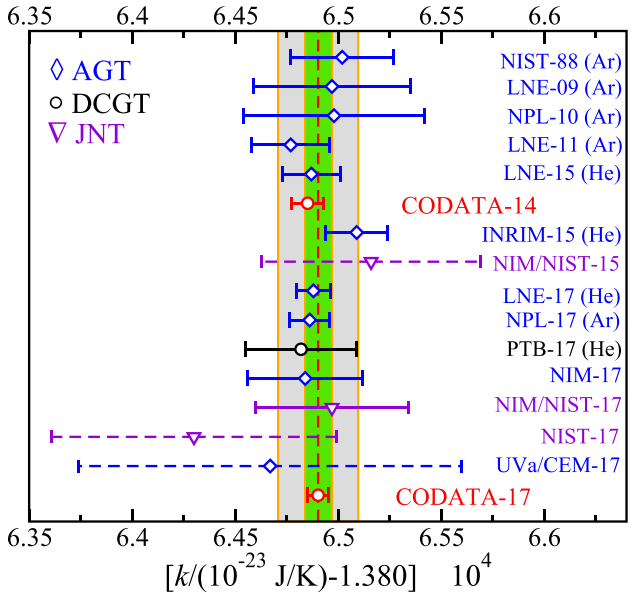

Figure 3. Values of the Boltzmann constant k inferred from the input data in table 4, the CODATA 2014 value, and the CODATA 2017 value in chronological order from top to bottom (see table 11). Dashed values were not included in the final 2017 adjustment. The inner green band is ± 5 parts in 10^7 and the outer grey band is ± 15 parts in 10^7. AGT: acoustic gas thermometry; DCGT: dielectric constant gas thermometry; JNT: Johnson noise thermometry.

^{4}He, where k is inferred from the Clausius–Mossotti equation and a theoretical evaluation of the static electric polarizability of a helium atom, here listed as *B*58. In the remainder of this subsection we briefly describe the individual measurements and techniques.

The measurement of R by AGT involves determining the speed of sound in a gas, usually Ar or He, at a known temperature at or near the triple point of water $T_{\rm TPW}$ and at various pressures p, and extrapolating to $p = 0$. The speed of sound follows from a measurement of the acoustic resonant frequencies of a gas-filled cavity, or resonator, which can be cylindrical, spherical, or often quasispherical in the form of a triaxial ellipsoid. The precise dimensions of the cavity are usually determined by measuring their electromagnetic modes. Finally, the molar mass of the gas is required and involves measuring its isotopic composition and accounting for impurities, sometimes introduced by out-gassing from the walls.

The acoustic-gas-thermometry values of R numbered *B*55.1-*B*55.5 were discussed and used in the CODATA-14 adjustment. Measurement *B*55.6 at INRIM, Torino (Gavioso *et al* 2015) was the first competitive data point to appear after our closing deadline of the 2014 adjustment. They used a slightly-misaligned spherical copper resonator with an internal radius of 90 mm filled with helium. The quoted uncertainty for R is dominated ($\approx$90%) by their measurement of the speed of sound. Smaller (nearly-equal) contributions to the uncertainty are due to the uncertainties in the molar mass of the helium gas and its temperature. The six evaluations *B*55.1-*B*55.6 are not independent. We have employed the approach of Moldover *et al* (2015) to evaluate the covariances among these values. The covariances in the form of correlation coefficients are listed in table 5.

Input datum *B*55.7, labeled NIM-17, is based on combining five AGT measurements with argon carried out over the last five years at NIM, Beijing, with help from researchers at NIST, Gaithersburg. The individual data can be found in Lin *et al* (2013), Feng *et al* (2015), and Feng *et al* (2017). In all cases steel cylindrical resonators of different lengths rather than the more common spherical or quasispherical resonator were used. It is worth noting that in Feng *et al* (2017) resonator lengths were obtained from measurements of resonant microwave frequencies while in the earlier experiments lengths were obtained by two-color laser interferometry. Feng *et al* (2017) also carefully reviewed and updated as appropriate the values and uncertainty budgets of their previous values of R. In addition, they evaluated the covariances among the five values and calculated a weighted mean following the CODATA procedure given in appendix E of CODATA-98. This mean with $u_{\rm r} = 2.0 \times 10^{-6}$ is used in our special 2017 adjustment.

Recently reported by NPL, Teddington (Podesta *et al* 2017), item *B*55.8 corresponds to a revision of argon-based AGT measurements in a quasi-spherical cavity published in 2013 (de Podesta *et al* 2013) and 2015 (de Podesta *et al* 2015). It is updated for argon isotopic composition by using a novel sampling procedure from its storage cylinder, which eliminates any possibility of contamination. The sampling was repeated three times and the samples were examined with two different mass spectrometers. The spectrometer measurements were traceable to gravimetrically prepared argon samples. The end result is a fractional increase of 5.0 parts in 10^7 in the molar mass of the argon compared to that found by de Podesta *et al* (2015) leading to a fractional increase of 7.1 parts in 10^7 for R with uncertainty $u_{\rm r} = 7.0 \times 10^{-7}$. This value is labeled NPL-17 in table 4 and supersedes the AGT datum NPL-13 in CODATA-14.

Item *B*55.9 is an AGT measurement at LNE, La Plaine-St. Denis (Pitre *et al* 2017). Three older AGT values of R by LNE are given in table 4. Datum *B*55.4 used argon, while all others used ^{4}He. The 2017 helium experiment employed a copper quasispherical triaxial ellipsoid resonator with a volume of about 3 L and a radius of 90 mm and was, in nearly equal parts, limited by uncertainties in the determination of temperature and acoustic resonances. This result has the smallest uncertainty $u_{\rm r} = 6.0 \times 10^{-7}$ of any of the 14 data that contribute to the determination of k.

We have included the four LNE values for R as separate input data rather than using their weighted mean also given in Pitre *et al* (2017) in order to account for correlations noted by Moldover *et al* (2015). Nevertheless, the weighted mean of the four LNE values including their correlation coefficients as given in tables 4 and 5 agrees with the weighted mean given by Pitre *et al* (2017).

Item *B*55.10, UVa/CEM-17, was determined in a joint project of the University of Valladolid, Valladolid, Spain, and the National Metrology Institute of Spain, Centro Español de Metrologia (CEM), Madrid. Reported by Segovia *et al* (2017), this AGT experiment used purified Ar gas and a steel ellipsoidal cavity of nominal 40 mm radius formed from two hemispheres bolted together and operated at $T_{\rm TPW}$. Their inside walls were coated with a 1.5 μm layer of gold. Acoustic transducers in the lower hemisphere and microwave transducers in

the upper hemisphere enabled simultaneous measurements of the acoustic and microwave frequencies.

A determination of the isotopic composition of the argon gas was not possible, so the UVa/CEM researchers used the results from Lee *et al* (2006) for the isotopic composition for Ar in atmospheric air and included additional components of uncertainty to account for possible impurities in the argon employed in the experiment and deviations of its isotopic composition from that of argon in air. The two largest contributors by far to their total relative uncertainty are the 4.7×10^{-6} uncertainty of the mean cavity radius and the 4.4×10^{-6} uncertainty of the measured frequencies of the acoustic modes.

The Johnson noise thermometry (JNT) method of determining k is discussed in CODATA-14 and is based on the Nyquist theorem $\langle U^2 \rangle = 4kTR_J\Delta f$, where $\langle U^2 \rangle$ is the Johnson noise voltage in a frequency bandwidth Δf across a resistance R_J at temperature T. For frequencies f less than 10 MHz and temperatures greater than 250 K this theorem holds with a fractional uncertainty significantly less than 1×10^{-6}, well below current experimental uncertainties.

The constant determined in JNT is the kelvin-hertz conversion factor k/h, when the noise voltage is measured in terms of the conventional value of the Josephson constant K_{J-90} and the resistance in terms of the conventional value of the von Klitzing constant R_{K-90}. In practice, the measured quantity is the ratio S_R/S_Q, where S_R is the thermal noise power spectral density of the resistor and S_Q is the pseudo noise power spectral density of approximately equal power synthesized by a pulsed-bias Josephson junction array also known as a quantum voltage noise source. The uncertainty of current JNT experiments is limited by statistics.

Item *B*56.1, NIM/NIST-15, in table 4 is a JNT measurement reported by Qu *et al* (2015), and was used in the 2014 final adjustment. This joint NIM-NIST thermometry project has continued and an improved value for k/h, item *B*56.2, NIM/NIST-17, was recently reported by Qu *et al* (2017). Some important changes were made to the apparatus, for example, the 200 Ω resistor was replaced with a 100 Ω resistor to increase the measurement bandwidth as were the leads used to connect the resistor and Josephson junction array to the measurement electronics. Nevertheless, the reduction in relative uncertainty is mainly the result of decreasing the statistical uncertainty by increasing the integration time from 33 d to 100 d. Based on the uncertainty budgets for NIM/NIST-15 and NIM/NIST-17 given by Qu *et al* (2017), the correlation coefficient between the two experiments is 0.021.

Item *B*56.3, NIST-17, is the JNT value of k/h determined at NIST, Boulder, reported by Flowers-Jacobs *et al* (2017). This is the latest result of continued work at NIST over the last decade. The most significant improvement is the input circuitry from the two noise sources to the measurement system amplifiers and the method employed to match the frequency responses of the two sources. The reported result with $u_r = 5.0 \times 10^{-6}$ is based on 49 d of data taking.

Item *B*57, PTB-17, is a multi-year effort of PTB, Berlin, to accurately measure the Boltzmann constant using dielectric constant gas thermometry (DCGT) of a ^{4}He gas. The method relies on the virial expansion of the equation of state and the Clausius–Mossotti equation to find an expression for $A_\epsilon(^4\text{He})/R$, the ratio of the molar polarizability of a ^{4}He gas and the molar gas constant R, in terms of the measurable relative dielectric constant $\epsilon_r = \epsilon(^4\text{He})/\epsilon_0$ at a known temperature T and various pressures p, and extrapolating to $p = 0$ (see CODATA-14).

The Boltzmann constant is then obtained from the equation $A_\epsilon(^4\text{He})/R = \alpha_0(^4\text{He})/(3\epsilon_0 k)$, where $\alpha_0(^4\text{He})$ is the static electric polarizability of a helium atom in SI units. It is equal to $4\pi\epsilon_0 a_0^3 \alpha_0^*(^4\text{He})$, where a_0 is the Bohr radius and $\alpha_0^*(^4\text{He})$ is the static electric polarizability of ^{4}He in atomic units. The latter is item *B*58 in table 4 calculated by Piszczatowski *et al* (2015) and also used in CODATA-14.

In the PTB experiments, carried out at T_{TPW}, the fractional change in capacitance of a specially constructed capacitor, first filled with helium gas at a known pressure and then without, is determined. Their first high-accuracy value for $A_\epsilon(^4\text{He})/R$ (Gaiser *et al* 2015) was used in CODATA-14. More recently, Gaiser *et al* (2017) reported results for two new capacitors, and a final value from the PTB DCGT project with $u_r = 1.9 \times 10^{-6}$ obtained by calculating the weighted mean of the values from the three capacitors and their covariances. The value for PTB-17, item *B*57 in table 4, was inadvertently omitted from Gaiser *et al* (2017) but was provided to the Task Group by Gaiser (2017).

For completeness we note that two other results relevant to the determination of k have recently been published. By measuring the optical refractive index of helium at a known temperature and pressure, Egan *et al* (2017) determined k with $u_r = 12.5 \times 10^{-6}$. Also, Urano *et al* (2017) determined k with $u_r = 10.2 \times 10^{-6}$ from JNT measurements using a superconducting circuit. However, their uncertainties are too large to be considered for inclusion in the 2017 Special Adjustment. The two results are consistent with the other Boltzmann constant data.

3.3.11. Tau mass and electroweak quantities. The mass of the tau lepton m_τ, the Fermi coupling constant G_F, and sine squared of the weak mixing angle $\sin^2\theta_W$, enter the calculation of the theoretical expression for the electron magnetic moment anomaly a_e. The values employed in the CODATA 2017 Special Adjustment are taken from the 2016 biennial report of the Particle Data Group (Patrignani *et al* 2016):

$$m_\tau c^2 = 1776.86(12)\ \text{MeV} \qquad [6.8 \times 10^{-5}], \tag{7}$$

$$\frac{G_F}{(\hbar c)^3} = 1.166\,3787(6) \times 10^{-5}\ \text{GeV}^{-2} \quad [5.1 \times 10^{-7}], \tag{8}$$

$$\sin^2\theta_W = 0.222\,90(30) \qquad [1.3 \times 10^{-3}]. \tag{9}$$

The definition $\sin^2\theta_W = 1 - (m_W/m_Z)^2$, where m_W and m_Z are, respectively, the masses of the $W^\pm$ and Z^0 bosons, is adopted because it is used in the calculation of the electroweak contributions to a_e (Czarnecki *et al* 1996). The value for the mass ratio given by the Particle Data Group (Patrignani *et al* 2016), $m_W/m_Z = 0.881\,53(17)$, leads to the above value of $\sin^2\theta_W$.

4. Analysis of data

There are 10 types of input data with two or more values and in general data of the same type agree among themselves; that is, the difference between any two data of the same type does not exceed the standard uncertainty of their difference $u_{\rm diff}$ by more than $2u_{\rm diff}$, or 2σ. However, there are two exceptions among the h data and one among the $N_{\rm A}$ data. Item *B*38.1 (NIST-98) differs from *B*38.4 (NRC-17) and from *B*38.5 (LNE-17) by 2.1σ and 2.2σ, respectively; and item *B*54.1 (IAC-11) and *B*54.3 (IAC-17) differ by 2.4σ.

The consistency between data of different kinds can be examined by comparing values of $A_{\rm r}({\rm p})$, α, h, and k that can be inferred from different kinds of experiments. Such inferred values are calculated from the indicated input datum and the datum's observational equation in table 7 using the 2017 Special Adjustment values of the constants as appropriate.

As can be seen from their respective observational equations in table 7, items *B*2 and *B*12, which are $A_{\rm r}(^1{\rm H})$ and $\omega_{\rm c}(^{12}{\rm C}^{6+})/\omega_{\rm c}({\rm p})$, determine $A_{\rm r}({\rm p})$. However, the two inferred values of $A_{\rm r}({\rm p})$ differ by 3.5σ.

The inferred values of α are compared in table 9 and figure 1, of h in table 10 and figure 2, and of k in table 11 and figure 3. The two values of α in table 9, the first from $a_{\rm e}$ (HarvU-08) and the second from $h/m(^{87}{\rm Rb})$ (LKB-11), differ by less than 2σ; and none of the 14 values of k in table 11 differs from another by as much as 2σ. However there are some differences greater than 2σ between XRCD inferred values of h and directly measured Kibble-balance values of h. The most significant of these are the differences between h from IAC-17 and the NIST-17, NRC-17, and NIST-15 values of h, which are 4.0σ, 2.8σ, and 2.7σ, respectively.

In summary, these comparisons have identified a few cases where data differ by significantly more than 2σ, implying that there may be input data with normalized residuals r_i with absolute values greater than two in least-squares calculations.

Our initial multivariate least-squares adjustment includes all of the input data in tables 2 and 4 and their correlation coefficients in tables 3 and 5. It is characterized by $N = 138$ input data, $M = 74$ adjusted constants, and $\nu = N - M = 64$ degrees of freedom; $\chi^2 = 72.9$, $p\,(\chi^2|\nu) = 0.21$, and Birge ratio $R_{\rm B} = \sqrt{\chi^2/\nu} = 1.07$. Five input data have $|r_i|$ greater than two. They are *B*2 in table 4, which is the AME2016 value of $A_{\rm r}(^1{\rm H})$; items *B*38.1 (NIST-98), *B*38.2 (NIST-15), and *B*38.3 (NIST-17), which are Kibble-balance values of h; and *B*54.3, an XRCD value of $N_{\rm A}$ (IAC-17); their values of $|r_i|$ are 3.3, 2.1, 2.1, 2.4, and 3.4, respectively.

To address these large residuals, we follow the usual CODATA Task-Group practice of reducing the absolute values of residuals to two or less by multiplying the uncertainties of the input data related to the problem by an expansion factor. If the data have covariances with other data, the covariances are multiplied by the same factor squared if the uncertainties of the other data are multiplied by the same expansion factor, or by only the expansion factor if the uncertainties of the other data with which they are correlated are not multiplied by the expansion factor. This ensures that the correlation coefficients of the data remain the same and the expansion factor does not significantly alter the values of the adjusted constants (variables) determined by the adjustment, only their uncertainties.

For the data that play the dominant role in determining the adjusted constant h, namely the Kibble-balance values of h, items *B*38.1-*B*38.5 (NIST-98, NIST-15, NIST-17, NRC-17, LNE-17), and the XRCD values of $N_{\rm A}$, items *B*54.1-*B*54.4 (IAC-11, IAC-15, IAC-17, NMIJ-17), an expansion factor of 1.7 brings all the Kibble balance and XRCD data into agreement. The relative uncertainties of the first five values of h in table 10 are, in parts in 10^9, only 15, 20, 23, 34, and 42, respectively.

The data that play the dominant role in determining the adjusted constant $A_{\rm r}({\rm p})$, namely *B*2 (AME-16) and *B*12 (MPIK-17), also require an expansion factor. Coincidentially it is 1.7 and reduces $|r_i|$ of *B*2 to 1.9.

We also follow the usual CODATA Task-Group practice of omitting data with self sensitivity coefficients $S_{\rm c}$ less than 1% in the final adjustment on which recommended values of constants are based (see section 2). Thus we delete input data *B*38.1 (NIST-98 value of h), *B*55.10 (UVa/CEM-17 value of R), and items *B*56.1 and *B*56.3 (NIM/NIST-15 and NIST-17 values of k/h), since their values of $S_{\rm c}$ are 0.43%, 0.30%, 0.88%, and 0.54%, respectively. With these items deleted and the two 1.7 expansion factors applied, the final adjustment on which the CODATA 2017 recommended values of h, e, k, and $N_{\rm A}$ are based is characterized by $N = 134$ input data, $M = 74$ adjusted constants, and $\nu = N - M = 60$ degrees of freedom; $\chi^2 = 43.5$, $p\,(\chi^2|\nu) = 0.95$, and Birge ratio $R_{\rm B} = \sqrt{\chi^2/\nu} = 0.85$.

5. Final results

The values for the constants h, e, k and $N_{\rm A}$ from the CODATA 2017 Special Adjustment are

$$h = 6.626\,070\,150(69) \times 10^{-34}\ {\rm J\ s} \quad [1.0 \times 10^{-8}]\,, \tag{10}$$

$$e = 1.602\,176\,6341(83) \times 10^{-19}\ {\rm C} \quad [5.2 \times 10^{-9}]\,, \tag{11}$$

$$k = 1.380\,649\,03(51) \times 10^{-23}\ {\rm J\ K^{-1}} \quad [3.7 \times 10^{-7}]\,, \tag{12}$$

$$N_{\rm A} = 6.022\,140\,758(62) \times 10^{23}\ {\rm mol^{-1}} \quad [1.0 \times 10^{-8}]\,. \tag{13}$$

Truncated and rounded values to provide the defining constants for the revised SI are (Newell *et al* 2018)

$$h = 6.626\,070\,15 \times 10^{-34}\ {\rm J\ s}, \tag{14}$$

$$e = 1.602\,176\,634 \times 10^{-19}\ {\rm C}, \tag{15}$$

$$k = 1.380\,649 \times 10^{-23}\ \mathrm{J\,K^{-1}}, \tag{16}$$

$$N_\mathrm{A} = 6.022\,140\,76 \times 10^{23}\ \mathrm{mol^{-1}}, \tag{17}$$

where it is understood that the units here are those of the revised SI. These values have been approved at the 106th meeting of the CIPM, with concurrence from its relevant consultative committees. The exact numerical values in equations (14)–(17) agree within the uncertainties with the adjusted numerical values in equations (10)–(13). The Consultative Committee for Thermometry recommended that eight digits be chosen for k; however, since the eighth digit is a zero, only seven digits are required (CCT 2017).

The CIPM notes that at the time of the adoption of the revision: the mass of the international prototype of the kilogram (IPK), $m(\mathcal{K})$, will be 1 kg with the same relative standard uncertainty as h in equation (10); the vacuum magnetic permeability μ_0 will be $4\pi \times 10^{-7}$ H m^{-1} with the same relative uncertainty as α in the Special Adjustment (2.3×10^{-10}); the thermodynamic temperature of the triple point of water will be 273.16 K with the same relative uncertainty as k in (12); and the molar mass of carbon 12 $M(^{12}\mathrm{C})$ will be 0.012 kg mol^{-1} with the same relative uncertainty as $N_\mathrm{A}h$ in the Special Adjustment (4.5×10^{-10}).

These expectations are indeed confirmed by the following considerations. In the case of the Planck constant and the IPK, Kibble balance measurements determine the constant C, in the relationship $h = Cm_\mathrm{d}(\mathcal{K})$, in terms of quantities with units that are the same before and after the redefinition, such as the local acceleration of gravity. The subscript d on the symbol for the IPK indicates that it is a defining quantity in the current SI with the value 1 kg. Similarly, x-ray-crystal-density measurements determine the constant D, in the relationship $h = Dm_\mathrm{d}(\mathcal{K})$, in terms of quantities with units that do not change in the redefinition and relatively accurately known constants that are unchanged by the redefinition. The adjusted value of h in (10) is a weighted mean of the various Kibble balances (labeled by i) and x-ray-crystal-density measurements (labeled by j) that yield values and uncertainties of C_i and D_j possibly with covariances. Just after the redefinition, the mass of the IPK will be an adjusted value based on the set of relations $m(\mathcal{K}) = C_i^{-1}h_\mathrm{d}$ and $m(\mathcal{K}) = D_j^{-1}h_\mathrm{d}$. In this case, h_d is the defining constant given in (14) and $m(\mathcal{K})$ is the adjusted quantity. Hence, the relative uncertainty of $m(\mathcal{K})$ will be the that of the set of quantities C_i^{-1} and D_j^{-1}, including their correlations, which is essentially the same as the uncertainty of h in equation (10).

For the quantity μ_0, we use the relationship $h/e^2 = (c/2\alpha)\mu_{0\mathrm{d}}$, where $\mu_{0\mathrm{d}}$ is the current defining constant for electrical quantities with its exact value. Just after the redefinition, the equation defining μ_0 is $\mu_0 = (2\alpha/c)h_\mathrm{d}/e_\mathrm{d}^2$, where e_d is the defining constant in (15). Thus its relative uncertainty is that of the adjusted value of α, which is the same as that of h/e^2.

In the case of the Boltzmann constant, the various measurements determine the constant F in the relationship $k = F/T_{\mathrm{TPWd}}$ where T_{TPWd} is the triple point of water and F is a quantity that depends on constants that do not change in the redefinition or whose changes are small compared to the uncertainties of the measurements. As in the case of mass, this relation can be inverted to yield $T_{\mathrm{TPW}} = F/k_\mathrm{d}$, where k_d is the defining constant in (16). Evidently the relative uncertainty of the derived value of T_{TPW} has the same relative uncertainty as k in (12).

For the molar mass of carbon, the relation $N_\mathrm{A}h = \left[cA_\mathrm{r}(\mathrm{e})\alpha^2/24R_\infty\right]M_\mathrm{d}(^{12}\mathrm{C})$, where $M_\mathrm{d}(^{12}\mathrm{C})$ is the exact defining constant 0.012 kg mol^{-1} in the current SI, gives $M(^{12}\mathrm{C}) = \left[cA_\mathrm{r}(\mathrm{e})\alpha^2/24R_\infty\right]^{-1}N_\mathrm{Ad}h_\mathrm{d}$, where N_Ad is the defining constant in (17) just after the redefinition. As in the cases above, the uncertainty in the determination of $M(^{12}\mathrm{C})$ is that of $N_\mathrm{A}h$ before the redefinition.

5.1. Proton radius 'puzzle'

The bound state proton and deuteron rms charge radii r_p and r_d obtained from Lamb shift measurements in muonic hydrogen and deuterium atoms ($\mathrm{p}\mu^-$, $\mathrm{d}\mu^-$) are not included in the 2017 Special Adjustment. The muonic hydrogen value of r_p is smaller than the H-D spectroscopic value and the e-p scattering value by 4.5σ and 3.5σ, respectively; see CODATA-14 for further discussion of this so called proton radius puzzle. The muonic deuterium result for r_d became available only last year and it is smaller than the H-D spectroscopic value by 5.0σ.

The muonic hydrogen and deuterium values are $r_\mathrm{p} = 0.840\,87(39)$ fm (Antognini *et al* 2013) and $r_\mathrm{d} = 2.125\,62(78)$ fm (Pohl *et al* 2016). If these are used in the final 2017 Special Adjustment in place of input data items $A51$ and $A52$ of table 2, then R_∞ decreases a fractional amount of about 5.3 times its u_r of 5.9×10^{-12}, or about 3.1 parts in 10^{11}. However, there are no changes in the exact numerical values for h, e, k, or N_A.

Acknowledgment

The Task Group gratefully acknowledges the help provided to it by the many colleagues throughout the world who provided results by the 1 July 2017 due-date and who answered questions both promptly and completely. The Task Group also thanks the General Conference on Weights and Measures (CGPM) for inviting it to play a significant role in the international effort to establish a revised SI for the 21st century.

List of symbols and abbreviations

ASD	NIST Atomic Spectra Database (online)
AMDC	Atomic Mass Data Center, transferred in 2013 to Institute of Modern Physics (IMP), Chinese Academy of Sciences, Lanzhou, PRC, from Centre de Spectrométrie Nucléaire et de Spectrométrie de Masse (CSNSM), Orsay, France
AME	Atomic mass evaluation from the AMDC (completed in year specified)
$A_\mathrm{r}(X)$	Relative atomic mass of X: $A_\mathrm{r}(X) = m(X)/m_\mathrm{u}$

a_e	Electron magnetic moment anomaly: $a_e = (\|g_e\| - 2)/2$
a_μ	Muon magnetic moment anomaly: $a_\mu = (\|g_\mu\| - 2)/2$
BIPM	International Bureau of Weights and Measures, Sèvres, France
BNL	Brookhaven National Laboratory, Upton, New York, USA
CEM	Centro Español de Metrologia, Madrid, Spain
CGPM	General Conference on Weights and Measures
CIPM	International Committee for Weights and Measures
CODATA	Committee on Data for Science and Technology of the International Council for Science
c	Speed of light in vacuum
d	Deuteron (nucleus of deuterium D, or ^{2}H)
e	Symbol for either member of the electron-positron pair; when necessary, e^- or e^+ is used to indicate the electron or positron
e	Elementary charge: absolute value of the charge of the electron
g_d	Deuteron g-factor: $g_d = \mu_d/\mu_N$
g_e	Electron g-factor: $g_e = 2\mu_e/\mu_B$
g_p	Proton g-factor: $g_p = 2\mu_p/\mu_N$
$g_X(Y)$	g-factor of particle X in the ground (1S) state of hydrogenic atom Y
HD	HD molecule (bound state of hydrogen and deuterium atoms)
h	Planck constant
$\hbar$	Reduced Planck constant: $h/2\pi$
HarvU	Harvard University, Cambridge, Massachusetts, USA
IAC	International Avogadro Coordination
INRIM	Istituto Nazionale di Ricerca Metrologica, Torino, Italy
K_J	Josephson constant: $K_J = 2e/h$
K_{J-90}	Conventional value of the Josephson constant K_J: $K_{J-90} = 483\,597.9$ GHz V^{-1}
k	Boltzmann constant: $k = R/N_A$
LAMPF	Clinton P. Anderson Meson Physics Facility at Los Alamos National Laboratory, Los Alamos, New Mexico, USA
LKB	Laboratoire Kastler-Brossel, Paris, France
LK/SY	LKB and SYRTE collaboration
LNE	Laboratoire national de métrologie et d'essais, Trappes and La Plaine-Saint-Denis, France
MIT	Massachusetts Institute of Technology, Cambridge, Massachusetts, USA
METAS	Federal Institute for Metrology, Bern-Wabern, Switzerland
MPIK	Max-Planck-Institut für Kernphysik, Heidelberg, Germany
MPQ	Max-Planck-Institut für Quantenoptik, Garching, Germany
$M(X)$	Molar mass of X: $M(X) = A_r(X)M_u$
Mu	Muonium (μ^+ e^- atom)
M_u	Molar mass constant: $M_u = 10^{-3}$ kg mol^{-1}
m_u	Unified atomic mass constant: $m_u = m(^{12}\mathrm{C})/12$
m_X, $m(X)$	Mass of X (for the electron e, proton p, and other elementary particles, the first symbol is used, i.e., m_e, m_p, etc.)
N_A	Avogadro constant
NIM	National Institute of Metrology, Beijing, PRC
NIST	National Institute of Standards and Technology, Gaithersburg, Maryland and Boulder, Colorado, USA
NMIJ	National Metrology Institute of Japan, Tsukuba, Japan
NPL	National Physical Laboratory, Teddington, UK
NRC	National Research Council of Canada, Measurement Science and Standards, Ottawa, Ontario, Canada
PTB	Physikalisch-Technische Bundesanstalt, Braunschweig and Berlin, Germany
p	Proton
QED	Quantum electrodynamics
$p(\chi^2\|\nu)$	Probability that an observed value of chi-square for ν degrees of freedom would by chance exceed χ^2
R	Molar gas constant
$\overline{R}$	Ratio of muon anomaly difference frequency to free proton NMR frequency
R_B	Birge ratio: $R_B = (\chi^2/\nu)^{\frac{1}{2}}$
r_d	rms charge radius of the deuteron
R_K	von Klitzing constant: $R_K = h/e^2$
R_{K-90}	Conventional value of the von Klitzing constant R_K: $R_{K-90} = 25\,812.807\ \Omega$
r_p	rms charge radius of the proton
R_∞	Rydberg constant: $R_\infty = m_e c\alpha^2/2h$
$r(x_i, x_j)$	Correlation coefficient of estimated values x_i and x_j: $r(x_i, x_j) = u(x_i, x_j)/[u(x_i)u(x_j)]$
S_c	Self-sensitivity coefficient
SI	Système international d'unités (International System of Units)
StPtrsb	Various institutions in St. Petersburg, Russian Federation
SYRTE	Systèmes de référence Temps Espace, Paris, France
T	Thermodynamic temperature
UMZ	Institut für Physik, Johannes Gutenberg Universität Mainz (or simply the University of Mainz), Mainz, Germany
USussex	University of Sussex, Brighton, UK
UVa	University of Valladolid, Valladolid, Spain
u	Unified atomic mass unit (also called the dalton, Da): 1 u $= m_u = m(^{12}\mathrm{C})/12$
u_{diff}	Standard uncertainty of the difference between two values (σ is sometimes used in place of u_{diff})
$u(x_i)$	Standard uncertainty (i.e., estimated standard deviation) of an estimated value x_i of a quantity X_i (also simply u)
$u_r(x_i)$	Relative standard uncertainty of an estimated value x_i of a quantity X_i: $u_r(x_i) = u(x_i)/\|x_i\|$, $x_i \neq 0$ (also simply u_r)
$u(x_i, x_j)$	Covariance of estimated values x_i and x_j
$u_r(x_i, x_j)$	Relative covariance of estimated values x_i and x_j: $u_r(x_i, x_j) = u(x_i, x_j)/(x_i x_j)$
WarsU	University of Warsaw, Warsaw, Poland
XROI	Combined x-ray and optical interferometer
YaleU	Yale University, New Haven, Connecticut, USA
α	Fine-structure constant: $\alpha = e^2/4\pi\epsilon_0\hbar c \approx 1/137$
$\Delta E_B(^A X^{n+})$	Energy required to remove n electrons from a neutral atom
$\Delta E_I(^A X^{i+})$	Electron ionization energies, $i = 0$ to $n - 1$
$\Delta\nu_{Mu}$	Muonium ground-state hyperfine splitting

δ_C	Additive correction to the theoretical expression for the electron ground-state g-factor in $^{12}C^{5+}$
δ_e	Additive correction to the theoretical expression for the electron magnetic moment anomaly a_e
δ_{Mu}	Additive correction to the theoretical expression for the ground-state hyperfine splitting of muonium $\Delta\nu_{Mu}$
δ_{Si}	Additive correction to the theoretical expression for the electron ground-state g-factor in $^{28}Si^{13+}$
$\delta_X(nL_j)$	Additive correction to the theoretical expression for an energy level of either hydrogen H or deuterium D with quantum numbers n, L, and j
ϵ_0	Electric constant (vacuum electric permittivity): $\epsilon_0 = 1/\mu_0 c^2$
$\doteq$	Symbol used to relate an input datum to its observational equation
μ	Symbol for either member of the muon-antimuon pair; when necessary, μ^- or μ^+ is used to indicate the negative muon or positive muon
μ_B	Bohr magneton: $\mu_B = e\hbar/2m_e$
μ_N	Nuclear magneton: $\mu_N = e\hbar/2m_p$
$\mu_X(Y)$	Magnetic moment of particle X in atom or molecule Y
μ_0	Magnetic constant (vacuum magnetic permeability): $\mu_0 = 4\pi \times 10^{-7}$ N/A^2
μ_X	Magnetic moment of particle X
ν	Degrees of freedom of a particular adjustment
$\nu(f_p)$	Difference between muonium hyperfine splitting Zeeman transition frequencies ν_{34} and ν_{12} at a magnetic flux density B corresponding to the free proton NMR frequency f_p
τ	Symbol for either member of the tau-antitau pair; when necessary, τ^- or τ^+ is used to indicate the negative tau or positive tau
χ^2	The statistic 'chi square'

References

Andreas B *et al* 2011 *Metrologia* **48** S1
Antognini A *et al* 2013 *Science* **339** 417
Aoyama T, Hayakawa M, Kinoshita T and Nio M 2015 *Phys. Rev.* D **91** 033006
Aoyama T, Hayakawa M, Kinoshita T and Nio M 2017 *Phys. Rev.* D **96** 019901
Azuma Y *et al* 2015 *Metrologia* **52** 360
Bartl G *et al* 2017 *Metrologia* **54** 693
CCU 2016 *Decision 8 of the 22nd Meeting of the Consultative Committee for Units* www.bipm.org/utils/common/pdf/CC/CCU/CCU22.pdf
CGPM 2011 *Resolution 1 of the 24th CGPM* www.bipm.org/en/CGPM/db/24/1/
CIPM 2015 *Decision CIPM/104-09 of the 104th CIPM, Session I* www.bipm.org/en/committees/cipm/meeting/104(I).html
CCT 2017 *Recommendation T1 of the 28th Consultative Committee for Thermometry (CCT) Meeting* www.bipm.org/utils/common/pdf/CC/CCT/CCT28.pdf
Czarnecki A, Krause B and Marciano W J 1996 *Phys. Rev. Lett.* **76** 3267
Czarnecki A and Szafron R 2016 *Phys. Rev.* A **94** 060501
Egan P F, Stone J A, Ricker J E, Hendricks J H and Strouse G F 2017 *Opt. Lett.* **42** 2944
Feng X J, Lin H, Gillis K A, Moldover M R and Zhang J T 2015 *Metrologia* **52** S343
Feng X J, Zhang J T, Lin H, Gillis K A, Mehl J B, Moldover M R, Zhang K and Duan Y N 2017 *Metrologia* **54** 748
Flowers-Jacobs N E, Pollarolo A, Coakley K J, Fox A E, Rogalla H, Tew W L and Benz S P 2017 *Metrologia* **54** 730
Fujii K, Massa E, Bettin H, Kuramoto N and Mana G 2018 *Metrologia* **55** L1
Gaiser C 2017 private communication
Gaiser C, Fellmuth B, Haft N, Kuhn A, Thiele-Krivoi B, Zandt T, Fischer J, Jusko O and Sabuga W 2017 *Metrologia* **54** 280
Gaiser C, Zandt T and Fellmuth B 2015 *Metrologia* **52** S217
Gavioso R M, Madonna Ripa D, Steur P P M, Gaiser C, Truong D, Guianvarc'h C, Tarizzo P, Stuart F M and Dematteis R 2015 *Metrologia* **52** S274
Haddad D, Seifert F, Chao L S, Li S, Newell D B, Pratt J R, Williams C and Schlamminger S 2016 *Rev. Sci. Instrum.* **87** 061301
Haddad D, Seifert F, Chao L S, Possolo A, Newell D B, Pratt J R, Williams C J and Schlamminger S 2017 *Metrologia* **54** 633
Hanneke D, Fogwell S and Gabrielse G 2008 *Phys. Rev. Lett.* **100** 120801
Heiße F *et al* 2017 *Phys. Rev. Lett.* **119** 033001
Huang W J, Audi G, Wang M, Kondev F G, Naimi S and Xu X 2017 *Chin. Phys.* C **41** 030002
Jegerlehner F 2017 private communication
Jentschura U D 2006 *Phys. Rev.* A **74** 062517
Kramida A, Ralchenko Y and Reader J 2017 *NIST Atomic Spectra Database Team* (Gaithersburg, MD: National Institute of Standards and Technology) https://physics.nist.gov/asd
Kuramoto N, Mizushima S, Zhang L, Fujita K, Azuma Y, Kurokawa A, Okubo S, Inaba H and Fujii K 2017 *Metrologia* **54** 716
Laporta S 2017 *Phys. Lett.* B **772** 232
Lee J-Y, Marti K, Severinghaus J P, Kawamura K, Yoo H-S, Lee J B and Kim J S 2006 *Geochim. Cosmochim. Acta* **70** 4507
Li Z *et al* 2017 *Metrologia* **54** 763
Lin H, Feng X J, Gillis K A, Moldover M R, Zhang J T, Sun J P and Duan Y Y 2013 *Metrologia* **50** 417
Mana G, Massa E, Sasso C P, Andreas B and Kuetgens U 2017 *Metrologia* **54** 559
Mohr P J, Newell D B and Taylor B N 2016 *Rev. Mod. Phys.* **88** 035009
Mohr P J, Newell D B and Taylor B N 2016 *J. Phys. Chem. Ref. Data* **45** 043102
Mohr P J and Taylor B N 2000 *Rev. Mod. Phys.* **72** 351
Mohr P J and Taylor B N 2005 *Rev. Mod. Phys.* **77** 1
Mohr P J, Taylor B N and Newell D B 2008 *Rev. Mod. Phys.* **80** 633
Mohr P J, Taylor B N and Newell D B 2008 *J. Phys. Chem. Ref. Data* **37** 1187
Mohr P J, Taylor B N and Newell D B 2012 *Rev. Mod. Phys.* **84** 1527
Mohr P J, Taylor B N and Newell D B 2012 *J. Phys. Chem. Ref. Data* **41** 043109
Moldover M R, Gavioso R M and Newell D B 2015 *Metrologia* **52** S376
Newell D B *et al* 2018 *Metrologia* in preparation (https://doi.org/10.1088/1681-7575/aa950a)
Patrignani C *et al* 2016 *Chin. Phys.* C **40** 1
Piszczatowski K, Puchalski M, Komasa J, Jeziorski B and Szalewicz K 2015 *Phys. Rev. Lett.* **114** 173004
Pitre L *et al* 2017 *Metrologia* **54** 856
de Podesta M, Underwood R, Sutton G, Morantz P, Harris P, Mark D F, Stuart F M, Vargha G and Machin G 2013 *Metrologia* **50** 354
de Podesta M, Yang I, Mark D F, Underwood R, Sutton G and Machin G 2015 *Metrologia* **52** S353

de Podesta M, Mark D F, Dymock R C, Underwood R, Bacquart T, Sutton G, Davidson S and Machin G 2017 *Metrologia* **54** 683
Pohl R *et al* 2016 *Science* **353** 669
Puchalski M, Komasa J and Pachucki K 2015 *Phys. Rev.* A **92** 020501
Qu J, Benz S P, Coakley K, Rogalla H, Tew W L, White R, Zhou K and Zhou Z 2017 *Metrologia* **54** 549
Qu J, Benz S P, Pollarolo A, Rogalla H, Tew W L, White R and Zhou K 2015 *Metrologia* **52** S242
Schlamminger S, Steiner R L, Haddad D, Newell D B, Seifert F, Chao L S, Liu R, Williams E R and Pratt J R 2015 *Metrologia* **52** L5
Segovia J J, Lozano-Martín D, Martin M C, Chamorro C R, Villamañán M A, Pérez E, García Izquierdo C and del Campo D 2017 *Metrologia* **54** 663
Thomas M, Espel P, Ziane D, Pinot P, Juncar P, Pereira Dos Santos F, Merlet S, Piquemal F and Genevès G 2015 *Metrologia* **52** 433
Thomas M, Ziane D, Pinot P, Karcher R, Imanaliev A, Pereira Dos Santos F, Merlet S, Piquemal F and Espel P 2017 *Metrologia* **54** 468
Urano C, Yamazawa K and Kaneko N H 2017 *Metrologia* **54** 847
Wang M, Audi G, Kondev F G, Huang W J, Naimi S and Xu X 2017 *Chin. Phys.* C **41** 030003
Williams E R, Steiner R L, Newell D B and Olsen P T 1998 *Phys. Rev. Lett.* **81** 2404
Wood B M, Sanchez C A, Green R G and Liard J O 2017 *Metrologia* **54** 399
Yerokhin V A and Harman Z 2017 *Phys. Rev.* A **95** 060501
Yerokhin V A and Shabaev V 2016 *Phys. Rev.* A **93** 062514
Yerokhin V A and Shabaev V M 2015 *Phys. Rev. Lett.* **115** 233002
Yost D C, Matveev A, Grinin A, Peters E, Maisenbacher L, Beyer A, Pohl R, Kolachevsky N, Hänsch T W and Udem T 2016 *Phys. Rev.* A **93** 042509
Zatorski J, Sikora B, Karshenboim S G, Sturm S, Köhler-Langes F, Blaum K, Keitel C H and Harman Z 2017 *Phys. Rev.* A **96** 012502